

---

# Massive stars as thermonuclear reactors and their explosions following core collapse

Alak Ray

Tata Institute of Fundamental Research, Mumbai 400 005, India [akr@tifr.res.in](mailto:akr@tifr.res.in)

**Summary.** Nuclear reactions transform atomic nuclei inside stars. This is the process of stellar nucleosynthesis. The basic concepts of determining nuclear reaction rates inside stars are reviewed. How stars manage to burn their fuel so slowly most of the time are also considered. Stellar thermonuclear reactions involving protons in hydrostatic burning are discussed first. Then I discuss triple alpha reactions in the helium burning stage. Carbon and oxygen survive in red giant stars because of the nuclear structure of oxygen and neon. Further nuclear burning of carbon, neon, oxygen and silicon in quiescent conditions are discussed next. In the subsequent core-collapse phase, neutronization due to electron capture from the top of the Fermi sea in a degenerate core takes place. The expected signal of neutrinos from a nearby supernova is calculated. The supernova often explodes inside a dense circumstellar medium, which is established due to the progenitor star losing its outermost envelope in a stellar wind or mass transfer in a binary system. The nature of the circumstellar medium and the ejecta of the supernova and their dynamics are revealed by observations in the optical, IR, radio, and X-ray bands, and I discuss some of these observations and their interpretations.

**Keywords:** nuclear reactions, nucleosynthesis, abundances; stars: interiors; supernovae: general; neutrinos; circumstellar matter; X-rays: stars

## 1 Introduction

The sun is not commonly considered a star and few would think of stars as nuclear reactors. Yet, that *is* the way it is, and even our own world is made out of the “fall-out” from stars that blew up and spewed radioactive debris into the nascent solar system<sup>1</sup>.

Nuclear Astrophysics is the field concerning “the synthesis and Evolution of atomic nuclei, by thermonuclear reactions, from the Big Bang to the present.

---

<sup>1</sup> Lecture Notes on Kodai School on Synthesis of Elements in Stars; eds. Aruna Goswami & Eswar Reddy, Springer Verlag, 2009

What is the origin of the matter of which we are made?" [1]. Our high entropy universe resulting from the Big Bang, contains many more photons per particle of matter with mass, e.g. protons and neutrons. Because of the high entropy as the universe expanded, there was time to manufacture elements only upto helium and the major products of cosmic nucleosynthesis remained the light elements hydrogen and helium<sup>2</sup>. Stars formed from this primordial matter. They used these elements, hydrogen and helium as fuel to generate energy like a giant nuclear reactor<sup>3</sup>. In the process, the stars could shine and manufacture higher atomic number elements like carbon, oxygen, calcium and iron which we and our world are made of. The heavy elements are either dredged up from the core of the star to the surface of the star from which they are dispersed by stellar wind or directly ejected into the interstellar medium when a (massive) star explodes. The stardust is the source of heavy elements for new generation of stars and sun-like systems.

Our sun is *not* a massive star. It burns hydrogen in a set of nuclear reactions called the pp-chain, whereas the more massive stars *presently* burn their hydrogen by the so-called CNO-cycle<sup>4</sup>. Nevertheless, to put nuclear reactions in stars in perspective, we shall start with a discussion of how these reactions proceed within the sun. There is a correspondence between the evolutionary state of a star, its external appearance<sup>5</sup> and internal core conditions and the nuclear fuel it burns, – a sort of a mapping between the astronomers Hertzsprung-Russel diagram and the nuclear physicist's chart of the nuclide [4], until nuclear burning takes place on too rapid a time scale.

The problem of evolution of stars to their explosion and subsequent interaction with the circumstellar medium has many time scales (ranging from tens of milliseconds to tens of thousands of years) and macroscopic length scales (from dimensions effectively that of a white dwarf to that of a supernova remnant, i.e from few thousand kilometers to many tens of light years). The physics of supernova explosions is complex and diverse and in many parts, the explosion mechanism is still an unsolved problem. Even the constraining parameters and ingredients which makes the SN explode are still controver-

---

<sup>2</sup> Note however suggestions [5, 6] that early generation of stars called Pop III objects can also contribute to the abundance of  ${}^4\text{He}$  seen in the universe today and the entire helium may not be a product of big bang nucleosynthesis alone.

<sup>3</sup> Our sun is slowly burning hydrogen into helium and is presently not exactly the same when it just started burning hydrogen. It will appear different once it exhausts all hydrogen it *can* burn in its core. In other words, nuclear reactions in stellar interiors determine the life-cycle of stars, apart from providing them with internal power for heat and light and manufacturing all the heavier elements that the early universe could not.

<sup>4</sup> Note however that CN cycle may have driven an early stage convection in the young Sun.

<sup>5</sup> Astronomers classify stars according to their colors and (absorption) line spectra and luminosities. Meghnad Saha showed [2, 3] the link between the classification scheme and temperature (and thermal ionization) of stellar atmosphere.

sial (see e.g. the discussion in [96]). It is possible that the identification of the key aspects in the explosion may require seminal observations about the conditions in the supernova core other than the indirect evidence such as explosion asymmetries, pulsar kicks or nucleosynthetic yields. Such observations may involve the future detection of strong neutrino signals and gravitational waves from a galactic supernova in future. Detectable neutrino signals from a supernova was seen in the case of SN 1987A, but since that target was in a neighboring satellite galaxy (the Large Magellanic Cloud), the number of neutrinos were too small to distinguish the fine points of theoretical issues.

Since nuclear astrophysics is not usually taught at the master's level nuclear physics specialization in our universities, these lecture notes are meant to be an introduction to the subject and a pointer to literature and Internet resources<sup>6</sup>. The emphasis in the first part of these lecture notes is on the nuclear reactions in the stars and how these are calculated, rather than how stars evolve. The latter usually forms a core area of stellar astrophysics.

This article is organized essentially in the same sequence that a massive star burns successively higher atomic number elements in its core, until it collapses and explodes in a supernova. The introductory part discusses how the rates of thermonuclear reactions in (massive) stars are calculated, what the different classes of reactions are and how the stars (usually) manage to burn their fuels so slowly<sup>7</sup>. The middle part describes the nuclear physics during the collapse phase of the massive star. The last part describes a few typical examples of what can be learned by optical, IR and X-ray studies about nucleosynthesis and dynamics of explosion in supernovae and supernova remnants such as Cassiopeia A, SN 1987A etc. Only core-collapse supernovae are discussed in these lectures, those that arise from massive stars (e.g. stars more massive than  $8M_{\odot}$  with typical solar metallicity at the time they start burn-

---

<sup>6</sup> See for example, [7] for a course of nuclear astrophysics, and the International Conference Proceedings under the title: "Nuclei in the Cosmos" for periodic research conferences in the field. Valuable nuclear astrophysics datasets in machine readable formats can be found at sites:[8], [9]. A new and updated version of the nuclear reactions rate library REACLIB for astrophysics is now being maintained as a public, web-based version at [10]. A complementary effort to develop software tools to streamline the process of getting the latest and best information into this new library is available at [11] (see [12]). Much of the material discussed in the first part of these notes can be found in textbooks in the subject, see e.g. [13], [14], [4], [15], [1] etc. There is also a recent book on the subject by Richard Boyd [16] that among other topics describes terrestrial and space born instruments operating in service to nuclear astrophysics. A Workshop on Solar fusion cross sections for the pp chain and CNO cycle held in 2009 by the Institute of Nuclear Theory is expected to result in a Reviews of Modern Physics article. Supernovae of various types are the sites where nuclear reactions in stars or explosions are of prime importance. For Internet resources to two recent Schools on these topics, see <http://icts.tifr.res.in/sites/Sgrb/Programme> and <http://www.tifr.res.in/~sn2004>.

<sup>7</sup> These issues were discussed in an earlier SERC School [17].

ing hydrogen in their cores, i.e. at the “Zero Age Main Sequence”, before any mass was lost from their surface). We shall not discuss the type Ia SNe<sup>8</sup> in these lectures. Abundance of elements in our galaxy Milky Way give important information about how stars affect the element and isotopic evolution in various parts of the galaxy. For a study of the evolution of elements from C to Zn in the galactic halo and disk, with yields of massive stars and type Ia SNe, see [20] and elsewhere in these Proceedings.

## 2 Stars and their thermonuclear reactions

While referring to Sir Ernest Rutherford “breaking down the atoms of oxygen and nitrogen”, Arthur Eddington remarked: “what is possible in the Cavendish Laboratory may not be too difficult in the sun” [21]. Indeed this is the case, but for the fact that a star does this by fusion reactions, rather than by transfer reactions, – in the process giving out heat and light and manufacturing fresh elements. Of all the light elements, hydrogen is the most important one in this regard, because: a) it has a large universal abundance, b) considerable energy evolution is possible with it because of the large binding energies of nuclei that can be generated from its burning and c) its small charge and mass allows it to penetrate easily through the potential barriers of other nuclei. A star burns its fuel in thermonuclear reactions in the core where the confinement of the fuel is achieved in the star’s own gravitational field. These reactions remain “controlled”, or self-regulated<sup>9</sup>, as long as the stellar material remains non-degenerate.

---

<sup>8</sup> The supernovae are classified by astronomers on the basis of their optical spectra at the time of their maximum light output. Those that do not show the presence of hydrogen in their spectra are classified as type I SNe. A subclass of them, type Ia’s are believed to arise from thermonuclear explosions in the electron degenerate cores of stars less massive than  $8M_{\odot}$  and are very useful to map the geometry of our universe, because they serve as calibratable “standard” candles. These “thermonuclear supernovae” are usually more luminous in the optical bands than the core-collapse varieties, but while the former class put out several MeVs of energy per nucleon, the core-collapse SNe or ccSNe, emit several *hundreds* of MeVs per nucleon from their *central engines* (mostly in down-scattered neutrinos). Apart from the missing hydrogen lines, the type Ia SNe show an absorption “trough” in their spectra around maximum light at 6150 Å, due to blue shifted Si II lines [18]. Of the other type I SNe which show no hydrogen and no Si II trough, some show helium in their early spectra (type Ib) and others have little or no helium and have a composition enhanced in oxygen (type Ic) [19]. These, (Ib and Ic) together with the type IIs constitute the core collapse SNe.

<sup>9</sup> There are however examples to the contrary when thermonuclear reactions take place in an explosive manner, e.g. when a whole white dwarf (resulting from an evolved intermediate mass star) undergoes merger with another and explodes, as nuclear fuel (carbon) is ignited under degenerate conditions, such as in a type Ia supernova; explosive thermonuclear reactions also take place in post-bounce core

The recognition of the quantum mechanical tunneling effect prompted Atkinson and Houtermans [22] to work out the qualitative treatment of energy production in stars. They suggested that the nucleus serves as both a cooking pot and a trap. Binding energy difference of four protons and two electrons (the nuclear fuel) and their ash, the helium nucleus, some 26.7 MeV is converted to heat and light that we receive from the sun<sup>10</sup>. The photons in the interior are scattered many a times, for tens of millions of years, before they reach the surface of the sun. Some of the reactions produce neutrinos, which because of their small cross-section for interaction, are not stopped or scattered by overlying matter, – but stream out straight from the core. Neutrinos are thus the best probes of the stellar core [23, 106], while the photons bear information from their surface of last scattering – the photosphere.

## 2.1 Why do the stars burn slowly: a look at Gamow peaks

The sun has been burning for at least 4.6 billion years<sup>11</sup>. How does it manage to burn so slowly<sup>12</sup>? Under the ambient conditions in the core, the relevant

---

collapse supernovae, when the hydrodynamic shock ploughs through unburnt Si- or O-layers in the mantle.

<sup>10</sup> Lord Kelvin surmised in the nineteenth century that the solar luminosity is supplied by the gravitational contraction of the sun. Given the solar luminosity, this immediately defined a solar lifetime (the so-called Kelvin-Helmholtz time):  $\tau_{KH} = GM_{\odot}^2/R_{\odot}L_{\odot} \sim \text{few} \times 10^7 \text{ yr}$ . This turned out to be much shorter than the estimated age of the earth at that time known from fossil records, and led to a famous debate between Lord Kelvin and the fossil geologist Cuvier. In fact, as noted above modern estimates of earth's age are much longer and therefore the need to maintain sunshine for such a long time requires that the amount of energy radiated by the sun during its lifetime is much larger than its gravitational energy or its internal (thermal) energy:  $L_{\odot} \times t_{\text{life}} \gg GM_{\odot}^2/R_{\odot}$ . This puzzle was resolved only later with the realization that the star can tap its much larger nuclear energy reservoir in its core through thermonuclear reactions. The luminosity of the sun however is determined by an interplay of atomic and gravitational physics that controls the opacity, chemical composition, the balance of pressure forces against gravity, etc. Nuclear physics determines how fast nuclear reactions go under under feedback control determined by the ambient conditions.

<sup>11</sup> Lord Rutherford [24] determined the age of a sample of pitchblende, to be 700 million years, by measuring the amount of uranium and radium and helium retained in the rock and by calculating the annual output of alpha particles. The oldest rock found is from Southwest Greenland:  $\approx 3.8 \text{ Gyr}$  old [15]. Radioactive dating of meteorites point to their formation and the solidification of the earth about  $4.55 \pm 0.07 \text{ years}$  ago [25]. Since the sun and the solar system formed only slightly before, their age at isolation and condensation from the interstellar medium is taken to be 4.6 Gyr [26].

<sup>12</sup> The Nobel prize citation of Hans Bethe (1967) who solved this problem, noted that this “ concerns an old riddle. How has it been possible for the sun to emit light and heat without exhausting its source not only during the thousands of

thermonuclear reaction cross sections are very small<sup>13</sup>. For reactions involving charged particles, nuclear physicists often encounter cross-sections near the Coulomb barrier of the order of millibarns. One can obtain a characteristic luminosity  $L_C$  based on this cross section and the nuclear energy released per reaction [15] :

$$L_C \sim \epsilon N \Delta E / \tau_C \quad (1)$$

where  $\epsilon \approx 10^{-2}$  is the fraction of total number of solar nuclei  $N \sim 10^{57}$  that take part in nuclear fusion reactions generating typically  $\Delta E \sim 25$  MeV in hydrogen to helium conversion. Here, the  $\tau_C$  is the characteristic time scale for reactions, which becomes minuscule for the cross-sections at the Coulomb barrier and the ambient density and relative speed of the reactants etc:

$$\tau_C \sim \frac{1}{n\sigma v} = \frac{10^{-8}s}{[n/(10^{26} \text{ cm}^{-3})][\sigma/1 \text{ mbarn}][v/10^9 \text{ cm s}^{-1}]} \quad (2)$$

This would imply a characteristic luminosity of  $L_c \approx 10^{20} L_\odot$ , even for a small fraction of the solar material taking part in the reactions (i.e.  $\epsilon \sim 10^{-2}$ ). If this was really the appropriate cross-section for the reaction, the sun would have been gone very quickly indeed. Instead the cross-sections are much less than that at the Coulomb barrier penetration energy (say at proton energies of 1 MeV), to allow for a long lifetime of the sun (in addition, weak-interaction process gives a smaller cross-section for some reactions than electromagnetic process, – see Section 3.1).

Stellar nuclear reactions can be either: a) charged particle reactions (both target and projectile are nuclei) or b) neutral particle (neutron) induced reactions. Both sets of reactions can go through either a resonant state of an intermediate nucleus or can be a non-resonant reaction. In the former reaction, the intermediate state could be a narrow unstable state, which decays into other particles or nuclei. In general, a given reaction can involve both

---

centuries the human race has existed but also during the enormously long time when living beings needing the sun for their nourishment have developed and flourished on our earth thanks to this source? The solution of this problem seemed even more hopeless when better knowledge of the age of the earth was gained. None of the energy sources known of old could come under consideration. A very important part of his work resulted in eliminating a great number of thinkable nuclear processes under the conditions at the center of the sun, after which only two possible processes remained..... (Bethe) attempted a thorough analysis of these and other thinkable processes necessary to make it reasonably certain that these processes, and only these, are responsible for the energy generation in the sun and similar stars. ”

<sup>13</sup> This makes the experimental verification of the reaction cross-sections a very challenging task, requiring in some cases, extremely high purity targets and projectiles so that relevant small event rates are not swamped by other reaction channels and products (see Rolfs and Rodney, Chapter 5 [13]).

types of reaction channels. In charged particle induced reactions, the cross-section for both reaction mechanisms drops rapidly with decreasing energy, due to the effect of the Coulomb barrier (and thus it becomes more difficult to measure stellar reaction cross-sections accurately). In contrast, the neutron induced reaction cross-section is very large and increases with decreasing energy (here, resonances may be superposed on a smooth non-resonant yield which follows the  $1/v \sim 1/\sqrt{E}$  dependence). These reaction rates and cross-sections can be then directly measured at stellar energies that are relevant (if such nuclei are long lived or can be generated). The schematic dependence of the cross-sections are shown in Fig. 1. We shall not discuss the neutron capture elements in these notes.

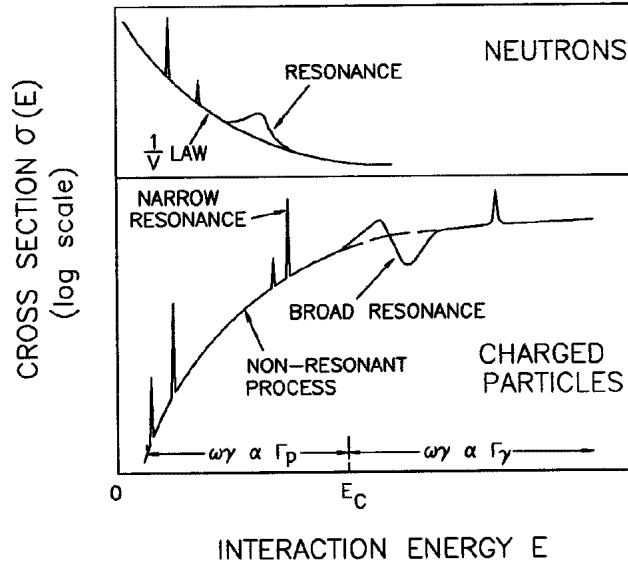


**Fig. 1.** Dependence of total cross-sections on the interaction energy for neutrons (top panel) and charged particles (bottom panel). Note the presence of resonances (narrow or broad) superimposed on a slowly varying non-resonant cross-section (after [13]).

## 2.2 Gamow peak and the astrophysical S-factor

The sun and other “main-sequence” stars (burning hydrogen in their core quiescently) evolve very slowly by adjusting their central temperature such that

the average thermal energy of a nucleus is small compared to the Coulomb repulsion an ion-ion pair encounters. This is how stars can live long for astronomically long times. A central temperature  $T \geq 10^7 \text{K}$  (or  $T_7 \geq 1$ , hereafter a subscript  $x$  to a quantity, indicates that quantity in units of  $10^x$ ) is required for sufficient kinetic energy of the reactants to overcome the Coulomb barrier and for thermonuclear reactions involving hydrogen to proceed at an effective rate, even though fusion reactions have positive  $Q$  values i.e. net energy is liberated out of the reactions. The classical turning point radius for a projectile of charge  $Z_2$  and kinetic energy  $E_p$  (in a Coulomb potential  $V_C = Z_1 Z_2 e^2 / r$ , and effective height of the Coulomb barrier  $E_C = Z_1 Z_2 e^2 / R_n = 550 \text{ keV}$  for a  $p + p$  reaction), is:  $r_{cl} = Z_1 Z_2 e^2 / E_p$ . Thus, classically a  $p + p$  reaction would proceed only when the kinetic energy exceeds 550 keV. Since the number of particles traveling at a given speed is given by the Maxwell Boltzmann (MB) distribution  $\phi(E)$ , only the tail of the MB distribution above 550 keV is effective when the typical thermal energy is 0.86 keV ( $T_9 = 0.01$ ). The ratio of the tails of the MB distributions:  $\phi(550 \text{ keV}) / \phi(0.86 \text{ keV})$  is quite minuscule, and thus classically at typical stellar temperatures this reaction will be virtually absent.

Although classically a particle with projectile energy  $E_p$  cannot penetrate beyond the classical turning point, quantum mechanically, one has a finite value of the squared wave function at the nuclear radius  $R_n : |\psi(R_n)|^2$ . The probability that the incoming particle penetrates the barrier is:

$$P = \frac{|\psi(R_n)|^2}{|\psi(R_c)|^2} \quad (3)$$

where  $\psi(r)$  are the wave-functions at corresponding points. Bethe [27] solved the Schroedinger equation for the Coulomb potential and obtained the transmission probability:-

$$P = \exp\left(-2KR_c \left[ \frac{\tan^{-1}(R_c/R_n - 1)^{1/2}}{(R_c/R_n - 1)^{1/2}} - \frac{R_n}{R_c} \right]\right) \quad (4)$$

with  $K = [2\mu/\hbar^2(E_c - E)]^{1/2}$ . This probability reduces to a much simpler relation at the low energy limit:  $E \ll E_c$ , which is equivalent to the classical turning point  $R_c$  being much larger than the nuclear radius  $R_n$ . The probability is:

$$P = \exp(-2\pi\eta) = \exp[-2\pi Z_1 Z_2 e^2 / (\hbar v)] = \exp[-31.3 Z_1 Z_2 (\frac{\mu}{E})^{1/2}] \quad (5)$$

where in the second equality,  $\mu$  is the reduced mass in Atomic Mass Units and  $E$  is the center of mass energy in keV. The exponential quantity involving the square brackets in the second expression is called the ‘‘Gamow factor’’. The reaction cross-section between particles of charge  $Z_1$  and  $Z_2$  has this exponential dependence due to the Gamow factor. In addition, because the

cross-sections are essentially “areas”: proportional to  $\pi(\lambda/2\pi\hbar)^2 \propto 1/E$ , it is customary to write the cross-section, with these two energy dependences filtered out:

$$\sigma(E) = \frac{\exp(-2\pi\eta)}{E} S(E) \quad (6)$$

where the factor  $S(E)$  is called the astrophysical S-factor. The S-factor may contain degeneracy factors due to spin, e.g.  $[(2J+1)/(2J_1+1)(2J_2+1)]$  as reaction cross-sections are summed over final states and averaged over initial states. Because the rapidly varying parts of the cross-section (with energy) are thus filtered out, the S-factor is a slowly varying function of center of mass energy, at least for the non-resonant reactions. It is thus much safer to extrapolate  $S(E)$  to the energies relevant for astrophysical environments from the laboratory data, which is usually generated at higher energies (due to difficulties of measuring small cross-sections), than directly extrapolating the  $\sigma(E)$ , which contains the Gamow transmission factor (see Fig. 2). Additionally, in order to relate  $\sigma(E)$  and  $S(E)$ , quantities measured in the laboratory to these relevant quantities in the solar interior, a correction factor  $f_0$  due to the effects of electron screening needs to be taken into account [28].

In the stellar core with a temperature  $T$ , reacting particles have many different velocities (energies) according to a Maxwell Boltzmann distribution:-

$$\phi(v) = 4\pi v^2 \left( \frac{\mu}{2\pi kT} \right)^{3/2} \exp\left[ -\frac{\mu v^2}{2kT} \right] \propto E^{1/2} \exp[-E/kT] \quad (7)$$

Nuclear cross-section or the reaction rates which also depend upon the relative velocity (or equivalently the center of mass energy) therefore need to be averaged over the thermal velocity (energy) distribution. Therefore, the thermally averaged reaction rate per particle pair is:

$$\langle \sigma v \rangle = \int_0^\infty \phi(v) \sigma(v) v dv = \left( \frac{8}{\pi\mu} \right)^{1/2} \frac{1}{(kT)^{3/2}} \int_0^\infty \sigma(E) E \exp(-E/kT) dE \quad (8)$$

The thermally averaged reaction rate per pair is, utilizing the astrophysical S-factor and the energy dependence of the Gamow-factor:

$$\langle \sigma v \rangle = \left( \frac{8}{\pi\mu} \right)^{1/2} \frac{1}{(kT)^{3/2}} \int_0^\infty S(E) \exp\left[ -\frac{E}{kT} - \frac{b}{\sqrt{E}} \right] dE \quad (9)$$

with  $b^2 = E_G = 2\mu(\pi e^2 Z_1 Z_2 / \hbar)^2 = 0.978\mu Z_1^2 Z_2^2$  MeV,  $E_G$  being called the Gamow energy. Note that in the expression for the reaction rate above, at low energies, the exponential term  $\exp(-b/\sqrt{E}) = \exp(-\sqrt{E_G/E})$  becomes very small whereas at high energies the Maxwell Boltzmann factor  $E^{1/2} \exp(-E/kT)$  vanishes. Hence there would be a peak (at energy, say,  $E_0$ ) of the integrand for the thermally averaged reaction rate per pair (see Fig. 3). The exponential part of the energy integrand can be approximated as:

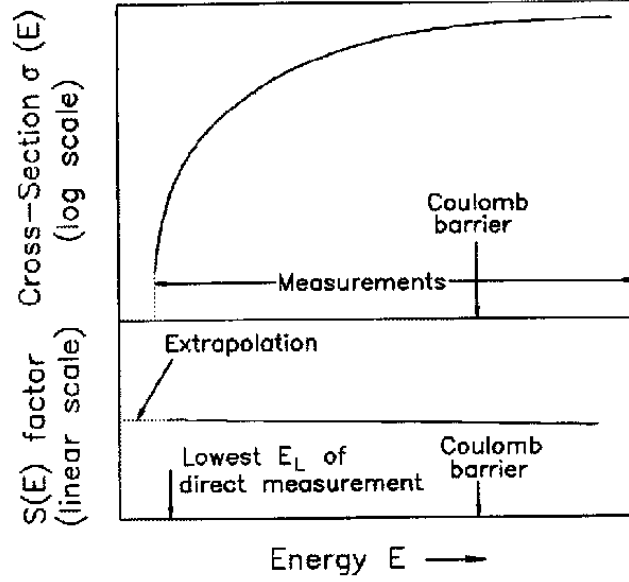


**Fig. 2.** Cross-section and astrophysical S-factor for charged particle reactions as a function of beam energy. The effective range of energy in stellar interiors is usually far less than the Coulomb barrier energy  $E_C$  or the lower limit  $E_L$  of laboratory measurements. The y-scale is logarithmic for cross-section but linear for S-factor; thus the cross section drops sharply in regions of astrophysical interest, while the change is much less severe for the S-factor. The extrapolation of laboratory data to lower energies relevant for astrophysical situations is more reliable for S-factor.

$$\exp\left[-\frac{E}{kT} - bE^{-1/2}\right] \sim C \exp\left[-\left(\frac{E - E_0}{\Delta/2}\right)^2\right] \quad (10)$$

where

$$C = \exp(-E_0/kT - bE_0^{-1/2}) = \exp(-3E_0/kT) = \exp(-\tau)$$

$$E_0 = (bkT/2)^{2/3} = 1.22\text{keV}(Z_1^2 Z_2^2 \mu T_6^2)^{1/3}$$

$$\Delta = 4(E_0 kT/3)^{1/2} = 0.75\text{keV}(Z_1^2 Z_2^2 A T_6^5)^{1/6}$$

Since most stellar reactions happen in a fairly narrow band of energies,  $S(E)$  will have a nearly constant value over this band averaging to  $S_0$ . With this, the reaction rate per pair of particles, turns out to be:

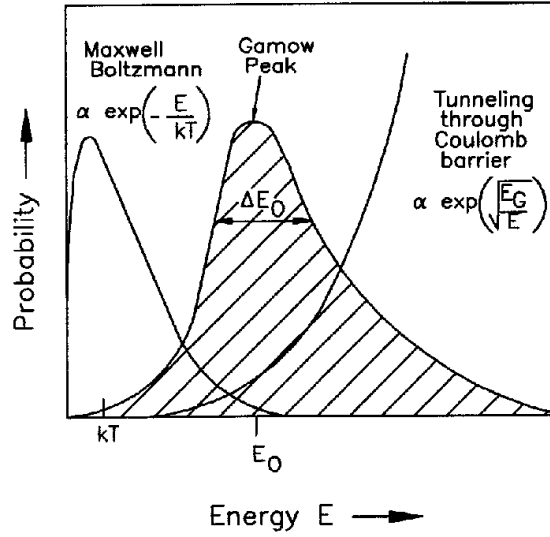


**Fig. 3.** The Gamow peak is a convolution of the energy distribution of the Maxwell Boltzmann probability and the quantum mechanical Coulomb barrier transmission probability. The peak in the shaded region near energy  $E_0$  is the Gamow peak that gives the highest probability for charged particle reactions to take place. Usually the Gamow peak is at a much higher energy than  $kT$ , and in the figure the ordinate scale (for the Gamow peak) is magnified with respect to those of the M-B and barrier penetration factors. See also Table 1.

$$\langle \sigma v \rangle = \left[ \frac{2}{kT} \right]^{\frac{3}{2}} \frac{S_0}{\pi \mu} \int_0^{\infty} e^{-\tau - 4 \left( \frac{E-E_0}{\Delta} \right)^2} dE = 4.510^{14} \frac{S_0}{AZ_1 Z_2} \tau^2 e^{-\tau} \text{cm}^3 \text{s}^{-1} \quad (11)$$

Here,

$$\tau = 3E_0/kT = 42.5(Z_1^2 Z_2^2 \mu / T_6)^{\frac{1}{3}} \quad (12)$$

The maximum value of the integrand in the above equation is:

$$I_{\max} = \exp(-\tau)$$

The values of  $E_0$ ,  $I_{\max}$ ,  $\Delta$ , etc., apart from the Coulomb barrier for several reactions are tabulated in Table 1 for  $T_6 = 15$ .

As the nuclear charge increases, the Coulomb barrier increases, and the Gamow peak  $E_0$  also shifts towards higher energies. Note how rapidly the maximum of the integrand  $I_{\max}$  decreases with the nuclear charge and the Coulomb barriers. The effective width  $\Delta$  is a geometric mean of  $E_0$  and  $kT$ , and  $\Delta/2$  is much less rapidly varying between reactions (for  $kT \ll E_0$ ). The rapid variation of  $I_{\max}$  indicates that of several nuclei present in the stellar core, those nuclear pairs will have the largest reaction rates, which have

the smallest Coulomb barrier. The relevant nuclei will be consumed most rapidly at that stage. (Note however that for the p+p reaction, apart from the Coulomb barrier, the strength of the weak force, which transforms a proton to a neutron also comes into play).

When nuclei of the smallest Coulomb barrier are consumed, there is a temporary dip in the nuclear generation rate, and the star contracts gravitationally until the temperature rises to a point where nuclei with the next lowest Coulomb barrier will start burning. At that stage, further contraction is halted. The star goes through well defined stages of different nuclear burning phases in its core dictated by the height of the Coulomb barriers of the fuels. Note also from the Table 1, how far  $E_0$ , the effective mean energy of reaction is below the Coulomb barrier at the relevant temperature. The stellar burning is so slow because the reactions are taking place at such a far sub-Coulomb region, and this is why the stars can last so long.

**Table 1.** Parameters of the thermally averaged reaction rates at  $T_6 = 15$ .

| Reaction                          | Coulomb<br>Barrier<br>(MeV) | Gamow<br>Peak ( $E_0$ )<br>(keV) | $I_{max}$<br>( $e^{-3E_0/kT}$ ) | $\Delta$<br>(keV) | $(\Delta)I_{max}$      |
|-----------------------------------|-----------------------------|----------------------------------|---------------------------------|-------------------|------------------------|
| p + p                             | 0.55                        | 5.9                              | $1.1 \times 10^{-6}$            | 6.4               | $7 \times 10^{-6}$     |
| p + N                             | 2.27                        | 26.5                             | $1.8 \times 10^{-27}$           | 13.6              | $2.5 \times 10^{-26}$  |
| $\alpha$ + C <sup>12</sup>        | 3.43                        | 56                               | $3 \times 10^{-57}$             | 19.4              | $5.9 \times 10^{-56}$  |
| O <sup>16</sup> + O <sup>16</sup> | 14.07                       | 237                              | $6.2 \times 10^{-239}$          | 40.4              | $2.5 \times 10^{-237}$ |

The above discussion assumes that a bare nuclear Coulomb potential is seen by the charged projectile. For nuclear reactions measured in the laboratory, the target nuclei are in the form of atoms with electron cloud surrounding the nucleus and giving rise to a screened potential – the total potential then goes to zero outside the atomic radius. The effect of the screening is to reduce the effective height of the Coulomb barrier. Atoms in the stellar interiors are in most cases in highly stripped state, and nuclei are immersed in a sea of free electrons which tend to cluster near the nucleus. When the stellar density increases, the so called Debye-Huckel radius  $R_D = (kT/4\pi e^2 \rho N_A \xi)^{1/2}$ , (here:  $\xi = \sum_i (Z_i^2 + Z_i) X_i / A_i$ ) which is a measure of this cluster “radius”, decreases, and the effect of shielding upon the reaction cross-section becomes more important. This shielding effect enhances thermonuclear reactions inside the star. The enhancement factor  $f_0 = \exp(0.188 Z_1 Z_2 \xi \rho^{1/2} T_6^{-3/2})$ , varies between 1 and 2 for typical densities and compositions [28] but can be large at high densities.

### 3 Hydrogen burning: the pp chain

The quantitative aspects of the problem of solar energy production with details of known nuclear physics of converting hydrogen into helium was first worked out by von Weizsäcker (1937-38) [32], [33] and Bethe & Critchfield (1938-1939) [34], which made it clear that two different sets of reactions : the p-p chains and the CN cycle can do this conversion. This happens in the core of the star initially (at the “main sequence” stage), and then later in the life of a star in a shell of burning hydrogen around an inert core of He.

In the first generation of stars in the galaxy only the p-p cycle may have operated. In second generation, heavier elements like C, N from the ashes of burning in previous stars are available and they too can act as catalysts to have thermonuclear fusion of hydrogen to helium. Since in the very first generation, the heavier elements like C, N were practically absent, all stars including the massive stars, burnt hydrogen through the p-p cycle. [A recent discovery ([35]) of a low-mass star with an iron abundance as low as 1/200,000 of the solar value (compare the previous record of lowest iron abundance less than 1/10,000 that of the sun), suggests that such first generation stars are still around].

The sun with a central temperature of 15.7 million degrees, ( $T_{6\odot}^c = 15.7$ ) burns by p-p chains. Slightly more massive star (with central temperature  $T_6 \geq 20$ ) burns H by the CNO cycle also. Davis et al.s’ solar neutrino experiment [23], which in 1968 had only an upper limit of the neutrino flux, itself put a limit of less than 9% of the sun’s energy is produced by the carbon-nitrogen cycle (the more recent upper limit [36] is 7.3%, from an analysis of several solar neutrino experiments, including the Kamland measurements). Note however that for the standard solar model, the actual contribution of CNO cycle to solar luminosity is  $\sim 1.5\%$  [15]). In CNO cycle, nuclei such as C, N, O serve as “catalysts” do in a chemical reaction. The pp-chain and the CNO cycle reaction sequences are illustrated in Figs. 4 and 10.

The pp-chain begins with the reaction  $p + p \rightarrow d + e^+ + \nu_e$ . Bethe and Critchfield [34] showed that weak nuclear reaction is capable of converting a proton into a neutron during the brief encounter of a scattering event. (This reaction overcomes the impasse posed by the instability of  ${}^2\text{He}$  in the  $p + p \rightarrow {}^2\text{He}$  reaction via the strong or electromagnetic interactions, and as the next nucleus  ${}^3\text{Li}$  reachable via these interactions is also unstable as a final product). Since a hydrogen atom is less massive than a neutron, such a conversion would be endothermic (requiring energy), except for the fact that a neutron in a deuterium nucleus  ${}^2\text{D}$  can form a bound state with the proton with a binding energy of 2.224 MeV – thus making the reaction exothermic with an available kinetic energy of 0.42 MeV. The released positron soon pair annihilates into photons making the total energy released to be 1.442 MeV.

Because of the low Coulomb barrier, in the p+p reaction ( $E_c = 0.55$  MeV), a star like the sun would have consumed all its hydrogen quickly (note the relatively large value of  $(\Delta)I_{max}$  in Table 1), were it not slowed down by the

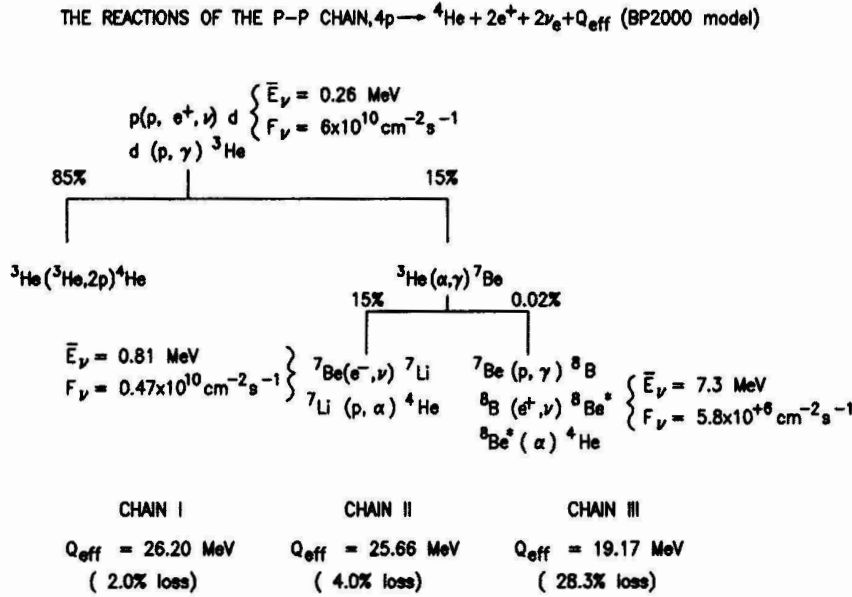


**Fig. 4.** The p-p chain starts with the formation of deuterium and  ${}^3\text{He}$ . Thereafter,  ${}^3\text{He}$  is consumed in the sun 85% of the time through ppI chain, whereas ppII and ppIII chains together account for 15% of the time in the Bahcall Pinsonneault 2000 solar model. The ppIII chain occurs only 0.02% of the time, but the  ${}^8\text{B}$   $\beta^+$ -decay provides the higher energy neutrinos (average  $\bar{E}_\nu = 7.3 \text{ MeV}$ ). The net result of the chains is the conversion of four protons to a helium, with the effective Q-values (reduced from 26.73 MeV) as shown, due to loss of energy in escaping neutrinos. See [38, 37] for updated branching ratios and neutrino fluxes for BPS2008(AGS) model.

weakness of the weak interactions. The calculation of probability of deuteron formation consists of two separate considerations: 1) the penetration of a mutual potential barrier in a collision of two protons in a thermal bath and 2) the probability of the  $\beta$ -decay and positron and neutrino emission. Bethe and Critchfield used the original Fermi theory (point interaction) for the second part, which is adequate for the low energy process.

### 3.1 Cross-section for deuterium formation

The total Hamiltonian  $H$  for the p-p interaction can be written as a sum of nuclear term  $H_n$  and a weak-interaction term  $H_w$ . As the weak interaction term is small compared to the nuclear term, first order perturbation theory can be applied and Fermi's "Golden rule", gives the differential cross-section as:

$$d\sigma = \frac{2\pi\rho(E)}{\hbar v_i} | \langle f | H_w | i \rangle |^2 \quad (13)$$

here  $\rho(E) = dN/dE$ , is the density of final states in the interval  $dE$  and  $v_i$  is the relative velocity of the incoming particles. For a given volume  $V$ , the number of states  $dn$  between  $p$  and  $p+dp$  is:-

$$dN = dn_e dn_\nu = \left( V \frac{4\pi p_e^2 dp_e}{h^3} \right) \left( V \frac{4\pi p_\nu^2 dp_\nu}{h^3} \right) \quad (14)$$

By neglecting the recoil energy of deuterium (since this is much heavier than the outgoing positron in the final state) and neglecting the mass of the electron neutrino, we have:

$$E = E_e + E_\nu = E_e + cp_\nu \quad (15)$$

and  $dE = dE_\nu = cp_\nu$ , for a given  $E_e$  and,

$$\rho(E) = dN(E)/dE = dn_e(dn_\nu/dE) = \frac{16\pi^2 V^2}{c^3 h^6} p_e^2 (E - E_e)^2 dp_e = \rho(E_e) dp_e \quad (16)$$

The matrix element that appears in the differential cross section, may be written in terms of the initial state wave function  $\Psi_i$  of the two protons in the entrance channel and the final state wave function  $\Psi_f$  as:

$$H_{if} = \int [\Psi_d \Psi_e \Psi_\nu]^* H_\beta \Psi_i d\tau \quad (17)$$

If the energy of the electron is large compared to  $Z \times$  Rydberg (Rydberg  $R_\infty = 2\pi^2 m e^4 / ch^3$ ), then a plane wave approximation is a good one:  $\Psi_e = 1/(\sqrt{V}) \exp(i\mathbf{k}_e \cdot \mathbf{r})$  where the wave-function is normalized over volume  $V$ . (For lower energies, typically 200 keV or less, the electron wave-function could be strongly affected by nuclear charge (see [39])). Apart from this, the final state wave function:  $[\Psi_d \Psi_e \Psi_\nu]$  has a deuteron part  $\Psi_d$  whose radial part rapidly vanishes outside the nuclear domain ( $R_0$ ), so that the integration need not extend much beyond  $r \simeq R_0$  (for example, the deuteron radius  $R_d = 1.7$  fm). Note that because of the Q-value of 0.42 MeV for the reaction, the kinetic energy of the electron ( $K_e \leq 0.42$  MeV) and the average energy of the neutrinos ( $\bar{E}_\nu = 0.26$  MeV) are low enough so that for both electrons and neutrino wave-functions, the product  $kR_0 \leq 2.2 \times 10^{-3}$  and the exponential can be approximated by the first term of the Taylor expansion:

$$\Psi_e = 1/(\sqrt{V}) [1 + i(\mathbf{k}_e \cdot \mathbf{r})] \sim 1/(\sqrt{V}) \quad (18)$$

and

$$\Psi_\nu \sim 1/(\sqrt{V})$$

Then the expectation value of the Hamiltonian, for a coupling constant  $g$  is:

$$H_{if} = \int [\Psi_d \Psi_e \Psi_\nu]^* H_\beta \Psi_i d\tau = \frac{g}{V} \int [\Psi_d]^* \Psi_i d\tau \quad (19)$$

The  $d\tau$  integration can be broken into space and spin parts  $M_{space}$  and  $M_{spin}$ :

$$d\sigma = \frac{2\pi}{\hbar v_i} \frac{16\pi^2}{c^3 \hbar^6} g^2 M_{spin}^2 M_{space}^2 p_e^2 (E - E_e)^2 dp_e \quad (20)$$

The total cross-section upto an electron energy of  $E$  is proportional to:

$$\int_0^E p_e^2 (E - E_e)^2 dp_e = \frac{(m_e c^2)^5}{c^3} \int_1^W (W_e^2 - 1)^{1/2} (W - W_e)^2 W_e dW_e \quad (21)$$

where  $W = (E + m_e c^2)/m_e c^2$ . The integral over  $W$  can be shown as:

$$f(W) = (W^2 - 1)^{1/2} \left[ \frac{W^4}{30} - \frac{3W^2}{20} - \frac{2}{15} \right] + \frac{W}{4} \ln[W + (W^2 - 1)^{1/2}] \quad (22)$$

so that:

$$\sigma = \frac{m_e^5 c^4}{2\pi^3 \hbar^7} f(W) g^2 M_{space}^2 M_{spin}^2 \quad (23)$$

At large energies, the factor  $f(W)$  behaves as:

$$f(W) \propto W^5 \propto \frac{1}{30} E^5 \quad (24)$$

The final state nucleus (deuterium in its ground state) in the reaction:  $p + p \rightarrow d + e^+ + \nu_e$ , has  $J_f^\pi = 1^+$ , with a predominant relative orbital angular momentum  $l_f = 0$  and  $S_f = 1$  (triplet S-state). For a maximally probable super-allowed transition, there is no change in the *orbital* angular momentum between the initial and final states of the nuclei. Hence for such transitions, the initial state two protons in the  $p + p$  reaction must have  $l_i = 0$ . Since the protons are identical particles, Pauli principle requires  $S_i = 0$ , so that the total wave-function will be antisymmetric in space and spin coordinates. Thus, we have a process:  $|S_i = 0, l_i = 0\rangle \rightarrow |S_f = 1, l_f = 0\rangle$ . This is a pure Gamow-Teller<sup>14</sup> transition with coupling constant  $g = C_A$  (the axial vector coupling component can be obtained, from the pure GT decay  ${}^6\text{He}(0^+) \rightarrow {}^6\text{Li}(1^+)$ ).

<sup>14</sup> In the beta-decay *allowed* approximation, we neglect the variation of the lepton wave-functions over the nuclear volume and the nuclear momentum (this is equivalent to neglecting all total lepton orbital angular momenta  $L > 0$ ). The total angular momentum carried off by the leptons is their total spin: i.e.  $S = 1$  or  $0$ , since each lepton has  $\frac{s=1}{2}$ . When the lepton spins in the final state are anti-parallel,  $s_e + s_\nu = s_{tot} = 0$  the process is the Fermi transition with Vector coupling constant  $g = C_V$  (e.g. a pure Fermi decay:  ${}^{14}\text{O}(J_i^\pi = 0^+) \rightarrow {}^{14}\text{N}(J_f^\pi = 0^+)$ ). When the final state lepton spins are parallel,  $s_e + s_\nu = s_{tot} = 1$ , the process is Gamow-

The spin matrix element in the above expression for energy integrated cross-section  $\sigma$ , is obtained from summing over the final states and averaging over the initial states *and* dividing by 2 to take into account that we have two identical particles in the initial state. Thus,

$$\lambda = \frac{1}{\tau} = \frac{m^5 c^4}{2\pi^3 \hbar^7 v_i} f(W) g^2 \frac{M_{space}^2 M_{spin}^2}{2} \quad (25)$$

where,  $M_{spin}^2 = \frac{(2J+1)}{(2J_1+1)(2J_2+1)} = 3$ . And the space matrix element is:

$$M_{space} = \int_0^\infty \chi_f(r) \chi_i(r) r^2 dr \quad (26)$$

in units of  $\text{cm}^{3/2}$ . The above integral contains the radial parts of the nuclear wave-functions  $\chi(r)$ , and involves Coulomb wave-functions for barrier penetration at (low) stellar energies. The integral has been evaluated by numerical methods ([42]), and Fig. 5 shows schematically how the  $M_{space}$  is evaluated for the overlap of the deuterium ground state wave-function with the initial pair of protons state. (See also [43], [44] for details of calculations of the overlap integral and writing the astrophysical S-factor in terms the beta decay rate of the neutron [43] which takes into account of radiative corrections to the axial-vector part of the neutron decay through an effective matrix

---

Teller with  $g = C_A$ . For Fermi coupling, there is no change in the (total) angular momentum between the initial and final states of the nuclei ( $\Delta J = 0$ ). For the Gamow-Teller coupling, the selection rules are:  $\Delta J = 0$  or  $\pm 1$  (but the possibility  $\Delta J = 0$  is excluded between two states of zero angular momentum). The size of the matrix element for a transition depends on the overlap of the wave-functions in the initial and final states. In the case of “mirror pair” of nuclei (the nucleus  $A_Z = (2Z + 1)_Z$  is the mirror of the nucleus  $(2Z + 1)_{Z+1}$ ), the wave-functions are very much alike as shown through simple heuristic arguments [40]. For these nuclei,  $ft$ -values range from  $\sim 1000 - 5000$  and are called super-allowed transitions. For super-allowed transitions, which have maximum decay probabilities, there are no changes in the *orbital* angular momentum between the initial and final states of the nuclei. In the  $p + p \rightarrow D + e^+ + \nu_e$  reaction, the initial proton state is antisymmetric to an interchange of space and spin coordinates and the final deuteron is symmetric in this respect. (In fact when the two protons are in the S state (which is most favorable for their close approach), their spins will be anti-parallel (a singlet state) whereas the ground state of the deuteron is a triplet S state). If this were the complete description of the exchange symmetry properties of the Gamow-Teller transition (permitting a change of spin direction of the proton as it transforms to a neutron, changing the total spin by one unit) advocated here this would actually be forbidden. However in the use of configuration space in beta-decay process one must include isotopic spin as well. The  $^1S$  state of the two protons is symmetric to exchange of this coordinate, whereas the deuteron (consisting of both a proton and a neutron) function is antisymmetric in this coordinate. In the complete coordinate system the transition is from an initial antisymmetric state to another antisymmetric final state accompanied by a positron emission ([41]).

element, the assumption being that these are the same as that for the proton beta decay in the pp reaction above). In the overlap integral one needs only the S-wave part for the wave-function of the deuteron  $\psi_d$ , as the D-wave part makes no contribution to the matrix element [42], although its contribution to the normalization has to be accounted for. The wave-function of the initial two-proton system  $\psi_p$  is normalized to a plane wave of unit amplitude, and again only the S-wave part is needed. The asymptotic form of  $\psi_p$  (well outside the range of nuclear forces) is given in terms of regular and irregular Coulomb functions and has to be defined through quantities related to the S-wave phase shifts in p-p scattering data). The result is a minuscule total cross-section of  $\sigma = 10^{-47} \text{cm}^2$  at a laboratory beam energy of  $E_p = 1 \text{ MeV}$ , which cannot be measured experimentally even with milliampere beam currents.

The reaction  $p + p \rightarrow d + e^+ + \nu_e$  is a non-resonant reaction and at all energies the rate varies smoothly with energy (and with stellar temperatures), with  $S(0) = 3.8 \times 10^{-22} \text{ keV barn}$  and  $dS(0)/dE = 4.2 \times 10^{-24} \text{ barn}$ . At for example, the central temperature of the sun  $T_6 = 15$ , this gives:  $\langle \sigma v \rangle_{pp} = 1.2 \times 10^{-43} \text{ cm}^3 \text{ s}^{-1}$ . For density in the center of the sun  $\rho = 100 \text{ gm cm}^{-3}$  and an equal mixture of hydrogen and helium ( $X_H = X_{He} = 0.5$ ), the mean life of a hydrogen nucleus against conversion to deuterium is  $\tau_H(H) = 1/N_H \langle \sigma v \rangle_{pp} \sim 10^{10} \text{ yr}$ . This is comparable to the age of the old stars. The reaction is so slow primarily because of weak interactions and to a lesser extent due to the smallness of the Coulomb barrier penetration factor (which contributes a factor  $\sim 10^{-2}$  in the rate), and is the primary reason why stars consume their nuclear fuel of hydrogen so slowly. For a calculation of the weak capture of protons on protons using calculated wavefunctions obtained from modern, realistic high precision interactions, see [29]

### 3.2 Deuterium burning

Once deuterium is produced in the weak interaction mediated p + p reaction, the main way this is burnt in the sun turns out to be:



This is a non-resonant direct capture reaction to the  ${}^3\text{He}$  ground state with a Q-value of 5.497 MeV and  $S(0) = 2.5 \times 10^{-3} \text{ keV barn}$ . The angle averaged cross-sections measured as a function of proton + deuterium center of mass energy, where the capture transitions were observed in gamma-ray detectors at several angles to the incident proton beam direction, are well explained by the direct capture model (see Fig. 6 after [13]). The LUNA collaboration [31] has measured the cross section down to a 2.5 keV c.m. energy, well below the solar Gamow peak using a segmented Bismuth germanate (BGO) gamma-ray detector and found the S(E) factor to be in fair agreement with extrapolation of data at higher energies.

The reactions comprising the rest of the (three) pp-chains start out with the predominant product of deuterium burning:  ${}^3\text{He}$  (manufactured from  $d+p$

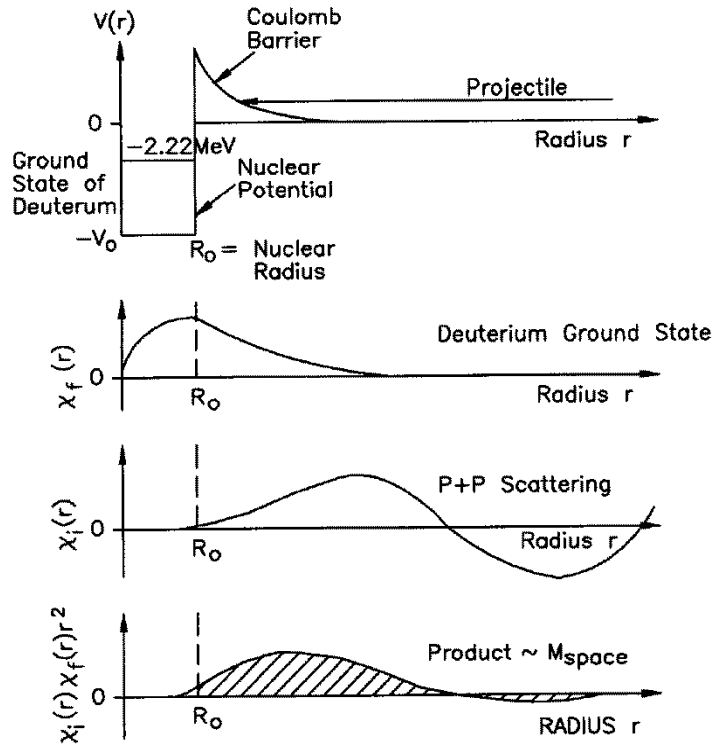


**Fig. 5.** Schematic representation (after [13]) of the numerical calculation of the spatial part of the matrix element  $M_{space}$  in the  $p + p \rightarrow d + e^+ + \nu_e$  reaction. The top part shows the potential well of depth  $V_0$  and nuclear radius  $R_0$  of deuterium with binding energy of  $-2.22$  MeV. The next part shows the radius dependence of the deuterium radial wave function  $\chi_d(r)$ . The wave-function extends far outside the nuclear radius with appreciable amplitude due to the loose binding of deuterium ground state. The p-p wave-function  $\chi_{pp}(r)$  which comprise the  $l_i = 0$  initial state has small amplitude inside the final nuclear radius. The radial part of the integrand entering into the calculation of  $M_{space}$  is a convolution of both  $\chi_d$  and  $\chi_{pp}$  in the second and third panels and is given with the hatched shading in the bottom panel. It has the major contribution far outside the nuclear radius.

reaction) as the starting point. The only other reactions with a  $S(0)$  greater than the above are:  $d(d, p)t$ ,  $d(d, n)^3He$ ,  $d(^3He, p)^4He$ , and  $d(^3He, \gamma)^5Li$ . However, because of the overwhelmingly large number of protons in the stellar thermonuclear reactors, the process involving protons on deuterium dominates. The rate of this reaction is so fast compared to its

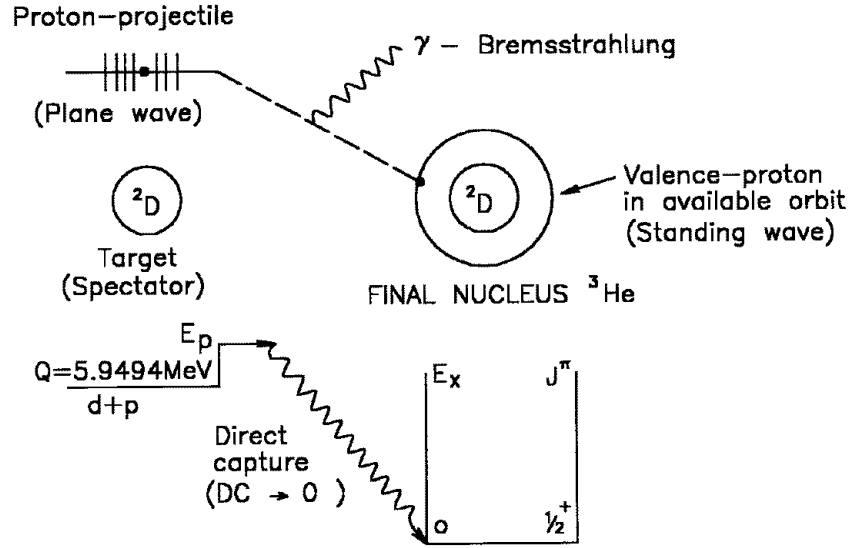


**Fig. 6.** The Direct Capture reaction  $d(p, \gamma)^3\text{He}$  to form  ${}^3\text{He}$  in its ground state. The proton projectile (shown as a plane wave) radiates away a bremsstrahlung photon to be captured in a “valence” orbital around the  ${}^2\text{D}$ .

precursor:  $p + p \rightarrow d + e^+ \nu_e$ , that the overall rate of the pp-chain is not determined by this reaction.

One can show that the abundance ratio of deuterium to hydrogen in a quasi-equilibrium has an extremely small value, signifying that deuterium is destroyed in thermonuclear burning. The time dependence of deuterium abundance  $D$  is:

$$\frac{dD}{dt} = r_{pp} - r_{pd} = \frac{H^2}{2} \langle \sigma v \rangle_{pp} - HD \langle \sigma v \rangle_{pd} \quad (28)$$

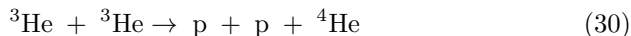
The self regulating system eventually reaches a state of quasi-equilibrium and has:

$$(D/H) = \langle \sigma v \rangle_{pp} / (2 \langle \sigma v \rangle_{pd}) = 5.6 \times 10^{-18} \quad (29)$$

at  $T_6 = 5$  and  $1.7 \times 10^{-18}$  at  $T_6 = 40$ . For the solar system however, this ratio is  $1.5 \times 10^{-4}$  and the observed  $(D/H)_{obs}$  ratio in the cosmos is  $\sim 10^{-5}$ . The higher cosmic ratio is due to primordial nucleosynthesis in the early phase of the universe before the stars formed. (The primordial deuterium abundance is a key quantity used to determine the baryon density in the universe). Stars only destroy the deuterium in their core due to the above reaction.

### 3.3 $^3\text{He}$ burning

The pp-chain-I is completed (see Fig. 4) through the burning of  $^3\text{He}$  via the reaction:



with an S-factor:  $S(0) = 5500$  keV barn and Q-value = 12.86 MeV. In addition, the reaction:



has an S-factor:  $S(0) = 6240$  keV barn, but since the deuterium concentration is very small as argued above, the first reaction dominates the destruction of  $^3\text{He}$  even though both reactions have comparable  $S(0)$  factors. The cross section for the former reaction near the Gamow energy for the sun, has been measured in [30].

$^3\text{He}$  can also be consumed by reactions with  $^4\text{He}$  (the latter is pre-existing from the gas cloud from which the star formed and is synthesized in the early universe and in Pop III objects). These reactions proceed through Direct Captures and lead to the ppII and ppIII parts of the chain (happening 15% of the time). Note that the reaction  $^3\text{He}(\alpha, \gamma)^7\text{Be}$  together with the subsequent reaction:  $^7\text{Be}(p, \gamma)^8\text{B}$  control the production of high energy neutrinos in the sun and are particularly important for the  $^{37}\text{Cl}$  solar neutrino detector constructed by Ray Davis and collaborators.

### 3.4 Reactions involving $^7\text{Be}$

As shown in Fig. 4, about 15% of the time,  $^3\text{He}$  is burned with  $^4\text{He}$  radiatively to  $^7\text{Be}$ . Subsequent reactions involving  $^7\text{Be}$  as a first step in alternate ways complete the fusion process:  $4\text{H} \rightarrow ^4\text{He}$  in the ppII and ppIII chains.

#### Electron capture process

The first step of the ppII chain is the electron capture reaction on  $^7\text{Be}$ :  $^7\text{Be} + e^- \rightarrow ^7\text{Li} + \nu_e$  (see Fig 7). This decay goes both to the ground state of  $^7\text{Li}$  as well as to its first excited state at  $E_X = 0.478$  keV,  $J^\pi = \frac{1}{2}^-$ ) – the percentage of decays to the excited state being 10.4 % in the laboratory. The energy released in the reaction with a Q-value of 0.862 keV is carried away by escaping mono-energetic neutrinos with energies:  $E_\nu = 862$  and 384 keV. The measured laboratory mean life of the decay is  $\tau = 76.9\text{d}$ . The capture rate in the laboratory can be obtained from Fermi's Golden Rule and utilizing the fact that the wave-functions of both the initial nucleus and the final one vanish rapidly outside the nuclear domain and the electron wave-function in that domain can be approximated as its value at  $r = 0$  and the neutrino wave-function by a plane wave normalizes to volume V, so that  $H_{if} =$

$\Psi_e(0)g/\sqrt{V} \int \Psi_{7Li}^* \Psi_{7Be} d\tau = \Psi_e(0)gM_n/\sqrt{V}$ , where  $M_n$  represents the nuclear matrix element and the resultant capture rate is:

$$\lambda_{EC} = 1/\tau_{EC} = (g^2 M_n^2 / \pi c^3 \hbar^4) E_\nu^2 |\Psi_e(0)|^2 \quad (32)$$

In the laboratory capture process, any of the various electron shells contribute to the capture rate; however the K-shell gives the dominant contribution. At temperatures inside the sun, e.g.  $T_6 = 15$ , nuclei such as  ${}^7Be$  are largely ionized. The nuclei however are immersed in a sea of free electrons resulting from the ionization process and therefore electron capture from continuum states is possible (see e.g., [45], [46]). Since all factors in the capture of continuum electrons in the sun are approximately the same as those in the case of atomic electron capture, except for the respective electron densities, the  ${}^7Be$  lifetime in a star,  $\tau_s$  is related to the terrestrial lifetime  $\tau_t$  by:

$$\frac{\tau_{fr}}{\tau_t} \sim \frac{2|\Psi_t(0)|^2}{|\Psi_{fr}(0)|^2} \quad (33)$$

where  $|\Psi_{fr}(0)|^2$  is the density of the free electrons  $n_e = \rho/m_H$  at the nucleus,  $\rho$  being the stellar density. The factor of 2 in the denominator takes care of the two spin states of calculation of the  $\lambda_t$  whereas the corresponding  $\lambda_{fr}$  is calculated by averaging over these two orientations. Taking account of distortions of the electron wave-functions due to the thermally averaged Coulomb interaction with nuclei of charge  $Z$  and contribution due to hydrogen (of mass fraction  $X_H$ ) and heavier nuclei, one gets the continuum capture rate as:

$$\tau_{fr} = \frac{2|\Psi_t(0)|^2 \tau_t}{(\rho/M_H)[(1 + X_H)/2] 2\pi Z \alpha (m_e c^2 / 3kT)^{1/2}} \quad (34)$$

with  $|\Psi_e(0)|^2 \sim (Z/a_0)^3/\pi$ . Bahcall et al [44] obtained for the  ${}^7Be$  nucleus a lifetime:

$$\tau_{fr}({}^7Be) = 4.72 \times 10^8 \frac{T_6^{1/2}}{\rho(1 + X_H)} \text{s}$$

The temperature dependence comes from the nuclear Coulomb field corrections to the electron wave-function which are thermally averaged. For solar condition the above rate [46] gives a continuum capture lifetime of  $\tau_{fr}({}^7Be) = 140d$  as compared to the terrestrial mean life of  $\tau_t = 76.9d$ . Actually, under stellar conditions, there is a partial contribution from some  ${}^7Be$  atoms which are only partially ionized, leaving electrons in the inner K-shell. So the contributions of such partially ionized atoms have to be taken into account. Under solar conditions the K-shell electrons from partially ionized atoms give another 21% increase in the total decay rate. Including this, gives the solar lifetime of a  ${}^7Be$  nucleus as:  $\tau_\odot({}^7Be) = 120d$ . In addition, the solar fusion reactions have to be corrected for plasma electrostatic screening enhancement effects. For a recent discussion of the issues see [47, 48].

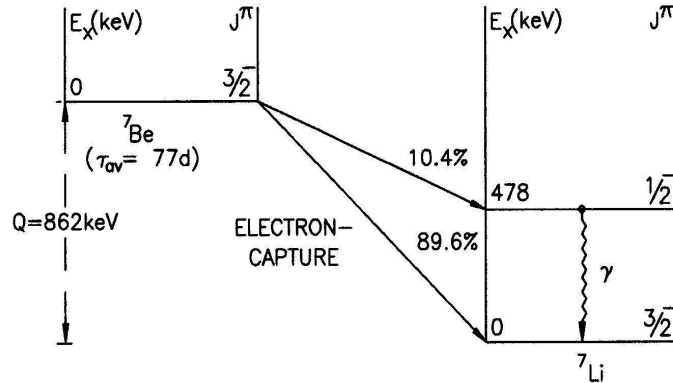
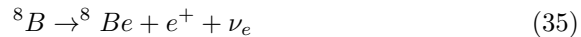


**Fig. 7.** Electron capture on  ${}^7\text{Be}$  nucleus. The capture proceeds 10.4% of the time to the first excited state of  ${}^7\text{Li}$  at 478 keV, followed by a decay to the ground state by the emission of a photon. The average energy of the escaping neutrinos (which are from the ppII chain) is 814 keV.

### Capture reaction leading to ${}^8\text{B}$

Apart from the electron capture reaction, the  ${}^7\text{Be}$  that is produced is partly consumed by proton capture via:  ${}^7\text{Be}(p, \alpha){}^8\text{B}$  reaction. Under solar conditions, this reaction happens only 0.02% of the time. The proton capture on  ${}^7\text{Be}$  proceeds at energies away from the 640 keV resonance via the direct capture process. Since the product  ${}^7\text{Li}$  nucleus emits an intense  $\gamma$ -ray flux of 478 keV, this prevents the direct measurement of the direct capture to ground state  $\gamma$ -ray yield. The process is studied indirectly by either the delayed positron or the breakup of the product  ${}^8\text{B}$  nucleus into two alpha particles. This reaction has a weighted average  $S(0) = 0.0238$  keVbarn [49]. The  ${}^7\text{Be}(p, \alpha){}^8\text{B}$  reaction cross section measurement has been attempted both by direct capture reactions as well as by the Coulomb dissociation of  ${}^8\text{B}$ . For a comparison of the  $S_{17}(0)$  factors determined by the two methods and a critical review of the differences of direct and indirect methods, see [50].

The product  ${}^8\text{B}$  is a radioactive nucleus with a lifetime  $\tau = 1.1$  s:

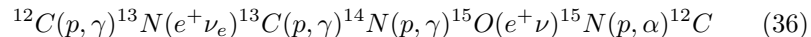


The positron decay of  ${}^8\text{B}(J^\pi = 2^+)$  goes mainly to the  $\Gamma = 1.6$  MeV broad excited state in  ${}^8\text{Be}$  at excitation energy  $E_x = 2.94$  MeV ( $J^\pi = 2^+$ ) due to the selection rules (see Fig. 8). This excited state has very short lifetime and quickly decays into two  $\alpha$ -particles. This completes the ppIII part of the pp-chain. The average energy of the neutrinos from  ${}^8\text{B}$  reactions is:  $\bar{E}_\nu({}^8\text{B}) = 7.3$  MeV. These neutrinos, having relatively high energy, play an important role in several solar neutrino experiments. The neutrino spectrum is not the same



with the capability to detect low energy neutrinos, this could in turn directly constrain the metallicity of the Sun's core<sup>15</sup>[38]. The early generation of stars (usually referred to as the Population II (Pop II) stars, although there is an even earlier generation of Pop III metal poor massive stars<sup>16</sup>) generated energy primarily through the pp-chain. The Pop II stars are still shining in globular clusters, and being of mass lower than that of the sun, are very old. Most other stars that we see today are later generation stars formed from the debris of heavier stars that contained heavy elements apart from (the most abundant) hydrogen. Thus in the second and third generation stars (which are slightly heavier than the sun) where higher central temperatures are possible because of higher gravity, hydrogen burning can take place through faster chain of reactions involving heavy elements C, N, and O which have some reasonable abundance (exceeding 1%) compared to other heavy elements like Li, Be, B which are extremely low in abundance. The favored reactions involve heavier elements (than those of the pp-chain) which have the smallest Coulomb barriers but with reasonably high abundance. Even though the Coulomb barriers of Li, Be, B are smaller than those of C, N, O (when protons are the lighter reactants (projectiles)), they lose out due to their lower abundance.

In 1937-1938, Bethe and von Weizsäcker independently suggested the CN part of the cycle, which goes as:



This has the net result, as before:  $4p \rightarrow {}^4\text{He} + 2e^+ + 2\nu_e$  with a  $Q = 26.73$ . In these reactions, the  ${}^{12}\text{C}$  and  ${}^{14}\text{N}$  act merely as catalysts as their nuclei are “returned” at the end of the cycle. Therefore the  ${}^{12}\text{C}$  nuclei act as seeds that can be used over and over again, even though the abundance of the seed material is minuscule compared to the hydrogen. But note that there is a loss of the catalytic material from the CN cycle that takes place through the  ${}^{15}\text{N}(p, \gamma){}^{16}\text{O}$  reactions. However, the catalytic material is subsequently returned to the CN cycle by the reaction:  ${}^{16}\text{O}(p, \gamma){}^{17}\text{F}(e^+ \nu_e){}^{17}\text{O}(p, \alpha){}^{14}\text{N}$ .

In the CN cycle (see Fig 10), the two neutrinos involved in the beta decays (of  ${}^{13}\text{N}$  ( $t_{1/2} = 9.97\text{min}$ ) and  ${}^{15}\text{O}$  ( $t_{1/2} = 122.24\text{s}$ )) are of relatively low energy and most of the total energy  $Q = 26.73$  MeV from the conversion of four protons into helium is deposited in the stellar thermonuclear reactor. The rate of the energy production is governed by the slowest thermonuclear reaction in the cycle. Here nitrogen isotopes have the highest Coulomb barriers in charged particle reactions, because of their  $Z = 7$ . Among them  ${}^{14}\text{N}(p, \gamma){}^{15}\text{O}$  is the

<sup>15</sup> A measurement CN-cycle neutrino flux (with an expected total flux of about  $5 \times 10^8 \text{ cm}^{-2} \text{ s}^{-1}$ ) would test an assumption of the Standard Solar Model that during the early pre-main-sequence Hayashi phase the Sun became homogeneous due to convective mixing and that subsequent evolution has not appreciably altered the distribution of metals [38].

<sup>16</sup> Though subsequently when Carbon has been synthesized by triple- $\alpha$  process, these Pop III stars turn on their CN cycle.

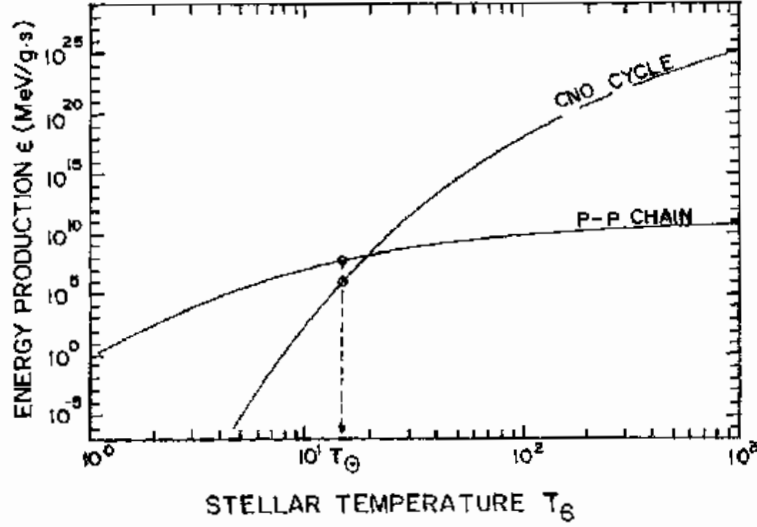


**Fig. 9.** Comparison of the temperature dependence of the p-p chain and the CNO cycle energy production. The points marked for the solar central temperature  $T_{\odot} = T_6 = 15.7$  are shown on both graphs. The CNO cycle generation dominates over the pp-chain at temperatures higher than  $T_6 = 20$ , so that for sun like stars, the pp-chain dominates. For more massive stars, the CNO cycle dominates as long as one of the catalysts: C, N, or O have initial mass concentration at least 1%. Note the logarithmic scales of the graph and how both rates drop sharply with decreasing temperature, with that of CNO cycle even more drastic due to higher Coulomb barriers.

slowest because this reaction having a final state photon is governed by electromagnetic forces while that involving the other nitrogen isotope:  $^{15}\text{N}(p, \alpha)^{12}\text{C}$  is governed by strong forces and is therefore faster.

From the CN cycle, there is actually a branching off from  $^{15}\text{N}$  by the reaction  $^{15}\text{N}(p, \gamma)^{16}\text{O}$  mentioned above. This involves isotopes of oxygen, and is called the ON cycle; finally the nitrogen is returned to the CN cycle through  $^{14}\text{N}$ . Together the CN and the ON cycles, constitutes the CNO bi-cycle. The two cycles differ considerably in their relative cycle-rates: the ON cycle operates only once for every 1000 cycles of the main CN cycle. This can be gauged from the  $S(0)$  factors of the two sets of reactions branching off from  $^{15}\text{N}$ : for the  $^{15}\text{N}(p, \alpha)^{12}\text{C}$  reaction  $S(0) = 65 \text{ MeV b}$ , whereas for  $^{15}\text{N}(p, \gamma)^{16}\text{O}$ , it is  $64 \text{ keV b}$ , i.e. a factor of 1000 smaller.

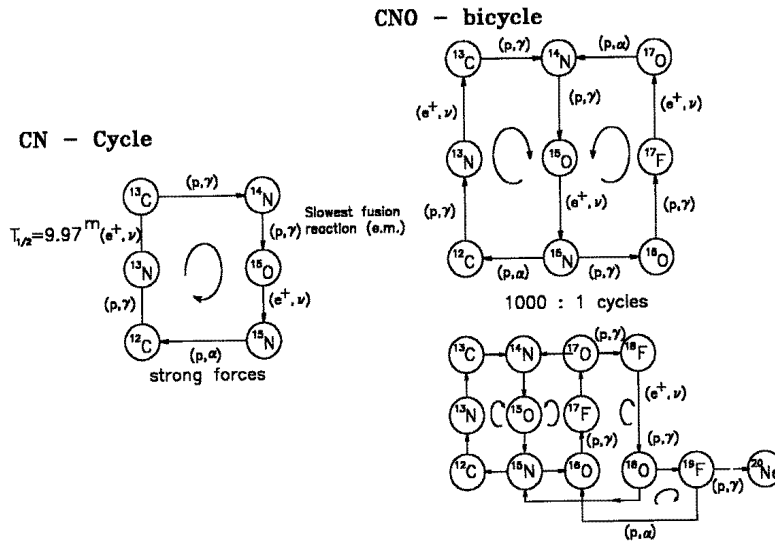


**Fig. 10.** The various CNO cycles. The left part is the CN cycle where only C and N serve as catalysts for the conversion of four protons into  $^4\text{He}$ . Here the slowest fusion reaction is  $(p,\gamma)$  reaction on  $^{14}\text{N}$  whereas the slower  $\beta$ -decay has a half-life of 9.97m. In the CNO bi-cycle (right part), there is leakage from the CN cycle to the ON cycle through the branching at  $^{15}\text{N}$ . The flow is returned to the CN cycle (which cycles 1000 times for each ON cycle) through  $^{17}\text{O}(p,\alpha)^{14}\text{N}$ . The right bottom part represents additional cycles linking into the CNO cycle through the  $^{17}\text{O}(p,\gamma)^{18}\text{F}$  reaction [13].

#### 4.1 Hot CNO and rp-process

The above discussion of CNO cycle is relevant for typical temperatures  $T_6 \leq 80$ . These are found in quiescently hydrogen burning stars with solar composition which are only slightly more massive than the sun. There are situations where the hydrogen burning takes place at temperatures ( $T \sim 10^8 - 10^9$  K) which are in excess of those found in the interiors of the ordinary “main sequence” stars. Examples of these are: hydrogen burning at the accreting surface of a neutron star or in the explosive burning on the surface of a white dwarf, i.e. novae, or the outer layers of a supernova shock heated material in the stellar mantle. These hot CNO cycles operate under such conditions on a rapid enough time scale (few seconds) so that even “normally”  $\beta$ -unstable nuclei like  $^{13}\text{N}$  will live long enough to be burned by thermonuclear charged particle reactions, before they are able to  $\beta$ -decay [52], [53]. So, unlike the normal CNO the amount of hydrogen to helium conversion in hot CNO is

limited by the  $\beta$ -decay lifetimes of the proton-rich nuclei like:  $^{14}\text{O}$  and  $^{15}\text{O}$  rather than the proton capture rate of  $^{14}\text{N}$ . Wallace and Woosley [54] showed that for temperatures,  $T \geq 5 \times 10^8 \text{K}$ , nucleosynthesised material can leak out of the cycles. This leads to a diversion from lighter to heavier nuclei and is known as the rapid proton capture or rp-process. The flow between the hot CNO cycle and the rp capture process in X-ray bursts from the atmosphere of a neutron star is regulated by the  $^{15}\text{O}(\alpha, \gamma)^{19}\text{Ne}$  reaction. Another alpha capture reaction  $^{18}\text{Ne}(\alpha, \gamma)^{21}\text{Na}$ , continuously processes the available  $^4\text{He}$  nuclei flowing towards heavier elements. For a recent discussion on the hot CNO and the rp process on accreting neutron stars, see [55].

The nucleosynthesis path of rp-process of rapid proton addition is analogous to the r-process of neutron addition (for neutron capture processes in the early galaxy see [56]). The hot hydrogen bath converts CNO nuclei into isotopes near the region of proton unbound nuclei (the proton drip line). For each neutron number, a maximum mass number  $A$  is reached where the proton capture must wait until  $\beta^+$ -decay takes place before the buildup of heavier nuclei (for an increased neutron number) can take place. Unlike the r-process the rate of the rp-process is increasingly hindered due to the increasing Coulomb barrier of heavier and higher- $Z$  nuclei to proton projectiles. Thus the rp-process does not extend all the way to the proton drip line but runs close to the beta-stability valley and runs through where the  $\beta^+$ -decay rate compares favorably with the proton captures.

## 5 Helium burning and the triple- $\alpha$ reaction

After hydrogen burning in the core of the star has exhausted its fuel, the helium core contracts slowly. Its density and temperature goes up as gravitational energy released is converted to internal kinetic energy. The contraction also heats hydrogen at the edge of the helium core, igniting the hydrogen to burn in a shell. At a still later stage in the star's evolution, the core has contracted enough to reach central temperature density conditions:  $T_6 = 100\text{--}200$  and  $\rho_c = 10^2 - 10^5 \text{ gm cm}^{-3}$  when the stellar core settles down to burn  $^4\text{He}$  in a stable manner. The product of helium burning is  $^{12}\text{C}$ . Since in nature, the  $A = 5$  and  $A = 8$  nuclei are not stable, the question arises as to how helium burning bridges this gap. A direct interaction of three  $\alpha$  particles to produce a  $^{12}\text{C}$  nucleus would seem at first sight, to be too improbable (as was mentioned, for example, in Bethe's 1939 paper [57], which was primarily on the CN cycle). However, Öpik [58] and Salpeter [43], [59] independently proposed a two step process where in the first step, two  $\alpha$  particles interact to produce a  $^8\text{Be}$  nucleus in its ground state (which is unstable to  $\alpha$ -breakup), followed by the unstable nucleus interacting with another  $\alpha$ -particle process to produce a  $^{12}\text{C}$  nucleus.

Thus the triple alpha reaction begins with the formation of  $^8\text{Be}$  that has a lifetime of only  $1 \times 10^{-16} \text{ s}$  (this is found from the width  $\Gamma = 6.8 \text{ eV}$  of the

ground state and is the cause of the  $A = 8$  mass gap). This is however long compared to the transit time  $1 \times 10^{-19}$  s of two  $\alpha$ -particles to scatter past each other non-resonantly with kinetic energies comparable to the Q-value of the reaction namely,  $Q = -92.1$  keV. So it is possible to have an equilibrium build-up of a small quantity of  ${}^8\text{Be}$  in equilibrium with its decay or reaction products:  $\alpha + \alpha \rightarrow {}^8\text{Be}$ . The equilibrium concentration of the  ${}^8\text{Be}$  nucleus can be calculated through the Saha equation

$$N_{12} = \frac{N_1 N_2}{2} \left( \frac{2\pi}{\mu kT} \right)^{3/2} \hbar^3 \frac{(2J+1)}{(2J_1+1)(2J_2+1)} \exp\left(-\frac{E_R}{kT}\right) \quad (37)$$

at the relevant temperature  $T_6 = 11$  and  $\rho = 10^5$  gm cm $^{-3}$  to be:

$$\frac{N({}^8\text{Be})}{N({}^4\text{He})} = 5.2 \times 10^{-10} \quad (38)$$

Salpeter suggested that this small quantity of  ${}^8\text{Be}$  serves as the seed for the second stage of the triple  $\alpha$ -capture into the  ${}^{12}\text{C}$  nucleus. It was however shown by Hoyle [61] that the amount of  ${}^{12}\text{C}$  produced for the conditions inside a star at the tip of the red-giant branch is insufficient to explain the observed abundance, *unless* the reaction proceeds through a resonance process [60]. The presence of such a resonance greatly speeds up the rate of the triple- $\alpha$  process which then proceeds through an s-wave ( $l = 0$ ) resonance in  ${}^{12}\text{C}$  near the threshold of  ${}^8\text{Be} + \alpha$  reaction. Since  ${}^8\text{Be}$  and  ${}^4\text{He}$  both have  $J^\pi = 0^+$ , an s-wave resonance would imply that the resonant state in question has to be  $0^+$  in the  ${}^{12}\text{C}$  nucleus. Hoyle suggested the excitation energy to be:  $E_X \sim 7.68$  MeV in the  ${}^{12}\text{C}$  nucleus and this state was experimentally found by W.A. Fowler's group ([62]) with spin-parity:  $J^\pi = 0^+$ . This state has a total width ([13])  $\Gamma = 8.9 \pm 1.08$  eV, most of which lies in  $\Gamma_\alpha$ , due to the major propensity of the  ${}^{12}\text{C}$  nucleus to break-up through  $\alpha$ -decay. (The decay of the excited state of  ${}^{12}\text{C}$  by  $\gamma$ -rays cannot go directly to the ground state, since the resonance state as well as the ground state of the  ${}^{12}\text{C}$  nucleus have both  $J^\pi = 0^+$  and  $0^+ \rightarrow 0^+$  decays are forbidden. This partial width due to gamma-decay is several thousand times smaller than that due to  $\alpha$ -decay). So,  $\Gamma = \Gamma_\alpha + \Gamma_{rad} \sim \Gamma_\alpha$  and  $\Gamma_{rad} = \Gamma_\gamma + \Gamma_{e^+e^-} = 3.67 \pm 0.50$  meV. Again the radiative width  $\Gamma_{rad}$  is dominated by the width due to photon width deexcitation:  $\Gamma_\gamma = 3.58 \pm 0.46$  meV. (Note the scales of *millielectron* Volts). The reaction scheme for the first and the second parts of the triple-alpha reaction is given in Fig. 11. The locations of the Gamow energy regions near the above resonance state (for several stellar temperatures) are shown only schematically.

The reaction rate for the  ${}^{12}\text{C}$  formation can be calculated by using the properties of the resonant state and the thermally averaged cross-section:

$$r_{3\alpha} = N_8 N_\alpha \langle \sigma v \rangle_{8\text{Be}+\alpha} \quad (39)$$

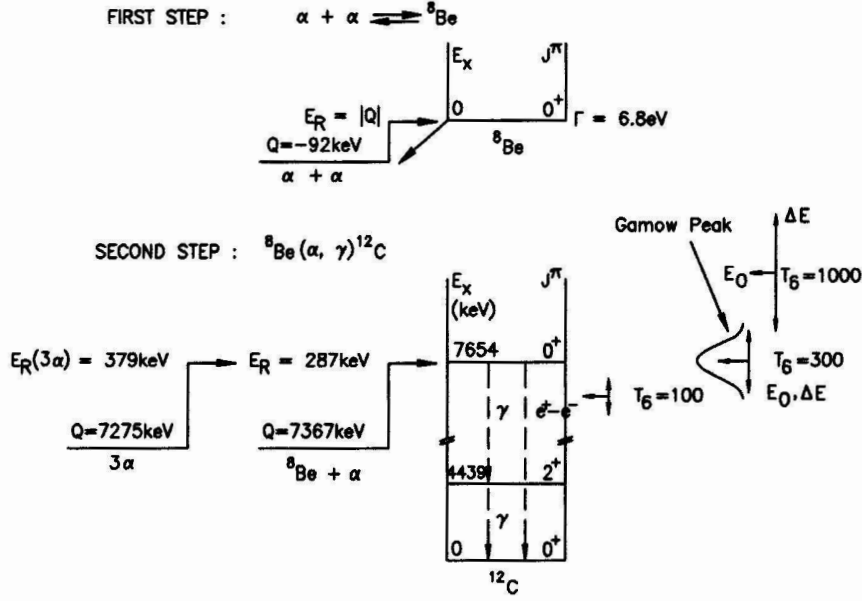


**Fig. 11.** Triple alpha process of  ${}^{12}\text{C}$  synthesis. In the first step a small amount of  ${}^8\text{Be}$  nuclei builds up in equilibrium with its decay products (forward and backward reactions involve alpha particles). The second step involves a capture of another alpha particle by the unstable  ${}^8\text{Be}$  nucleus which proceeds via an s-wave resonance state in the product nucleus  ${}^{12}\text{C}$  located close to the Gamow energy window for temperatures indicated schematically by the three-way arrows on the right.

Here  $N_{{}^8\text{Be}}$  and  $N_\alpha$  are the number densities of interacting  ${}^8\text{Be}$  and  ${}^4\text{He}$  nuclei and the angular brackets denote thermal averaging over a Maxwell Boltzmann distribution  $\psi(E)$ . This averaging leads to:

$$r_{3\alpha} = N_{{}^8\text{Be}}N_\alpha \int_0^\infty \psi(E)v(E)\sigma(E)dE \quad (40)$$

with

$$\psi(E) = \frac{2}{\sqrt{\pi}} \frac{E}{kT} \exp(-E/kT) \frac{dE}{(kTE)^{1/2}}$$

and

$$\sigma(E) = \pi \left( \frac{\lambda}{2\pi} \right)^2 \frac{2J+1}{(2J_1+1)(2J_2+1)} \frac{\Gamma_1\Gamma_2}{(E-E_R)^2 + (\Gamma/2)^2}$$

is the Breit-Wigner resonant reaction cross section with the resonant energy centroid at  $E = E_R$ . The total width  $\Gamma$  is a sum of all decay channel widths such as  $\Gamma_1 = \Gamma_\alpha$  and  $\Gamma_2 = \Gamma_\gamma$ . If the width  $\Gamma$  is only a few eVs then the

functions  $\psi(E)$  and  $v(E)$  can be pulled out of the integral. Then, the reaction rate will contain an integral like:  $\int_0^\infty \sigma_{BW}(E)dE = 2\pi(\lambda/2\pi\hbar)^2\omega\Gamma_1\Gamma_2/\Gamma$ , where  $\omega = (2J+1)/[(2J_1+1)(2J_2+1)]$  and the functions pulled out of the integral need to be evaluated at  $E = E_R$ . Since most of the time the excited state of the  $^{12}C^*$  breaks-up into  $\alpha$ -particles, we have  $\Gamma_1 = \Gamma_\alpha$  dominating over  $\Gamma_\gamma$  and  $(\Gamma_1\Gamma_2/\Gamma) \sim \Gamma_2$ . This limit usually holds for resonances of energy sufficiently high so that the incident particle width ( $\Gamma_1$ ) dominates the natural width of the state ( $\Gamma_2$ ). In that case, we can use the number density of the  $^8Be$  nuclei in equilibrium with the  $\alpha$ -particle nuclei bath as described by Saha equilibrium condition:

$$N(^8Be) = N_\alpha^2 \omega f \frac{h^3}{(2\pi\mu kT)^{3/2}} \exp(-E_r/kT) \quad (41)$$

where  $f$  is the screening factor. It is possible to get the overall triple-alpha reaction rate by calculating the equilibrium concentration of the excited (resonant) state of  $^{12}C$  reached by the  $^8Be + \alpha \rightarrow ^{12}C^*$  reaction and then multiplying that concentration by the gamma-decay rate  $\Gamma_\gamma/\hbar$  which leads to the final product of  $^{12}C$ . So, the reaction rate for the final step of the triple-alpha reaction turns out to be:

$$r_{3\alpha} = N_{^8Be} N_\alpha \hbar^2 \left( \frac{2\pi}{\mu kT} \right)^{3/2} \omega f \Gamma_2 \exp(-E_r'/kT) \quad (42)$$

where  $\mu$  is the reduced mass of the reactants  $^8Be$  and  $\alpha$  particle. This further reduces by the above argument to:

$$r_{3\alpha \rightarrow ^{12}C} = \frac{N_\alpha^3}{2} 3^{3/2} \left( \frac{2\pi\hbar^2}{M_\alpha kT} \right)^3 f \frac{\Gamma_\alpha \Gamma_\gamma}{\Gamma \hbar} \exp(-Q/kT) \quad (43)$$

The  $Q$ -value of the reaction is the sum of  $E_R(^8Be + \alpha) = 287$  keV and  $E_R(\alpha + \alpha) = |Q| = 92$  keV and turns out to be:  $Q_{3\alpha} = (M_{^{12}C^*} - 3M_\alpha)c^2 = 379.38 \pm 0.20$  keV [63]. Numerically, the energy generation rate for the triple-alpha reaction is:

$$\epsilon_{3\alpha} = \frac{r_{3\alpha} Q_{3\alpha}}{\rho} = 3.9 \times 10^{11} \frac{\rho^2 X_\alpha^3}{T_8^3} f \exp(-42.94/T_8) \text{ erg gm}^{-1} \text{ s}^{-1} \quad (44)$$

The triple alpha reaction has a very strong temperature dependence: near a value of temperature  $T_0$ , one can show that the energy generation rate is:

$$\epsilon(T) = \epsilon(T_0) \left( \frac{T}{T_0} \right)^n \quad (45)$$

where,  $n = 42.9/T_8 - 3$ . Thus at a sufficiently high temperature and density, the helium gas is very highly explosive, so that a small temperature rise gives rise to greatly accelerated reaction rate and energy liberation. When helium thermonuclear burning is ignited in the stellar core under degenerate conditions, an unstable and sometimes an explosive condition develops.

## 6 Survival of $^{12}\text{C}$ in red giant stars and $^{12}\text{C}(\alpha, \gamma)^{16}\text{O}$ reaction

The product of the triple-alpha reactions  $^{12}\text{C}$ , is burned into  $^{16}\text{O}$  by  $\alpha$ -capture reactions:



If this reaction proceeds too efficiently in helium burning Red giant stars, then all the carbon will be burned up to oxygen. Carbon is however the most abundant element in the universe after hydrogen, helium and oxygen, and the cosmic C/O ratio is about 0.6. In fact, the O and C burning reactions and the conversion of He into C and O take place in similar stellar core temperature and density conditions. Major ashes of He burning in Red Giant stars are C and O. Red Giants are the source of the galactic supply of  $^{12}\text{C}$  and  $^{16}\text{O}$ . Fortuitous circumstances of the energy level structures of these alpha-particle nuclei are in fact important for the observed abundance of oxygen and carbon.

For example, if as in the case of the  $3\alpha$  reaction, there was a resonance in the  $^{12}\text{C}(\alpha, \gamma)^{16}\text{O}$  reaction near the Gamow window for He burning conditions (i.e.  $T_9 \sim 0.1 - 0.2$ ), then the conversion of  $^{12}\text{C} \rightarrow ^{16}\text{O}$  would have proceeded at a very rapid rate. However, the energy level diagram of  $^{16}\text{O}$  shows that for temperatures upto about  $T_9 \sim 2$ , there is no level available in  $^{16}\text{O}$  to foster a resonant reaction behavior (Fig. 12). But since this nucleus is found in nature, its production must go through either: 1) a non-resonant direct capture reaction or 2) non-resonant captures into the tails of nearby resonances (i.e. sub-threshold reactions). In Fig. 12, also shown on the left of the  $^{16}\text{O}$  energy levels, is the threshold for the  $^{12}\text{C} + ^4\text{He}$  reaction, drawn at the appropriate level with respect to the ground state of the  $^{16}\text{O}$  nucleus. The Gamow energy regions drawn on the extreme right for temperatures  $T_9 = 0.1$  and above, indicates that for the expected central temperatures, the effective stellar (center of mass) energy region is near  $E_0 = 0.3$  MeV. This energy region is reached by the low energy tail of a broad resonance centered at  $E_{CM} = 2.42$  MeV above the threshold (the  $J^\pi = 1^-$  state at 9.58 MeV above the ground state of  $^{16}\text{O}$ ) with a (relatively large) resonance width of 400 keV. On the other hand, there are two sub-threshold resonances in  $^{16}\text{O}$  (at  $E_X = 7.12$  MeV and  $E_X = 6.92$  MeV), i.e. -45 keV and -245 keV *below* the  $\alpha$ -particle threshold that have  $J^\pi = 1^-$  and  $J^\pi = 2^+$ , that contribute to stellar burning rate by their high energy tails. However, electric dipole (E1)  $\gamma$ -decay of the 7.12 MeV state is inhibited by isospin selection rules. Had this not been the case, the  $^{12}\text{C}(\alpha, \gamma)^{16}\text{O}$  reaction would have proceeded fast and  $^{12}\text{C}$  would have been consumed during helium burning itself. The two sub-threshold states at -45 keV and -245 keV give contributions to the astrophysical S-factor of:  $S_{1^-}(E_0) = 0.1$  MeV barn and  $S_{2^+}(E_0) = 0.2$  MeV barn respectively at the relevant stellar energy  $E_0 = 0.3$  MeV. The state at  $E_{CM} = 2.42$  MeV ( $J^\pi = 1^-$  state at 9.58 MeV) gives a contribution:  $S_{1^-}(E_0) = 1.5 \times 10^{-3}$  MeV barn. The

total S-factor at  $E_0 = 0.3$  MeV is therefore close to 0.3 MeV barn. These then provide low enough S or cross-section to not burn away the  $^{12}\text{C}$  entirely to  $^{16}\text{O}$ , so that  $C/O \sim 0.1$  at the least.

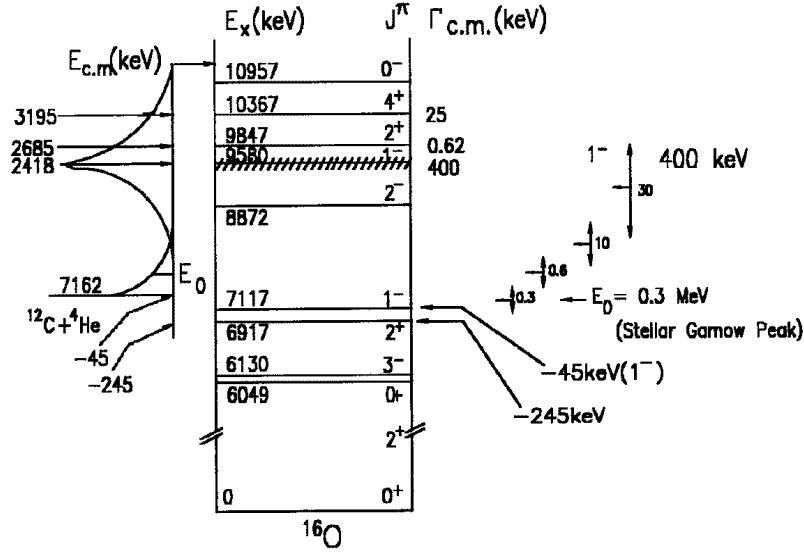


**Fig. 12.** Energy levels of  $^{16}\text{O}$  nucleus near and above the alpha-particle threshold of capture on  $^{12}\text{C}$ . Shown on the right are effective stellar energy regions corresponding to the temperatures given near the three-way arrows. The reaction rate is influenced mainly by the high energy tails of two sub-threshold resonances in  $^{16}\text{O}$  at  $E_R = -45$  keV and  $E_R = -245$  keV, plus the low energy tail of another high-lying broad resonance at 9580 keV.

Additionally,  $^{16}\text{O}$  nuclei are not burnt away by further  $\alpha$ -capture in the reaction:



A look at the level schemes of  $^{20}\text{Ne}$  (see Fig. 13) shows the existence of a  $E_X = 4.97$  MeV state ( $J^\pi = 2^-$ ) in the Gamow window. However, this state cannot form in the resonance reaction due to considerations of parity conservation (unnatural parity of the resonant state)<sup>17</sup>. The lower 4.25 MeV state ( $J^\pi = 4^+$ ) in  $^{20}\text{Ne}$  also cannot act as a sub-threshold resonance as it

<sup>17</sup> Whether or not a resonant state can be formed or accessed via a given reaction channel depends upon the angular momentum and parity conservation laws. The spins of the particles in the entrance channel,  $j_1, j_2$  and relative angular momen-

lies too far below threshold and is formed in the g-wave state. Therefore only direct capture reactions seem to be operative, which for  $(\alpha, \gamma)$  reactions lead to cross-sections in the range of nanobarns or below. Thus the destruction of  $^{16}\text{O}$  via:  $^{16}\text{O}(\alpha, \gamma)^{20}\text{Ne}$  reaction proceeds at a very slow rate during the stage of helium burning in Red Giant stars, for which the major ashes are carbon and oxygen and these elements have their galactic origin in the Red Giants.

To summarize, the synthesis of two important elements for the evolution of life as we know on the earth have depended upon fortuitous circumstances of nuclear properties and selection rules for nuclear reactions. These are: 1) the mass of the unstable lowest (ground) state of  $^8\text{Be}$  being close to the combined mass of two  $\alpha$ -particles; 2) there is a resonance in  $^{12}\text{C}$  at 7.65 MeV which enhances the alpha addition reaction (the second step); and 3) parity conservation has protected  $^{16}\text{O}$  from being destroyed in the  $^{16}\text{O}(\alpha, \gamma)^{20}\text{Ne}$  reactions by making the 4.97 MeV excited state in  $^{20}\text{Ne}$  of unnatural parity.

The experimental determination of the reaction rate  $^{12}\text{C}(\alpha, \gamma)^{16}\text{O}$  has been an important goal in nuclear astrophysics for several decades. Its cross section at the position of the Gamow window for a typical stellar temperature of  $2.5 \times 10^8\text{K}$  is comparable to that of weak interaction cross-sections. At those energies, this reaction is practically a non-resonant reaction and its cross-section is determined by the tails of interfering resonance and sub-threshold states [64]. The low cross section and the complexity of low energy contributions to the reaction rate makes a reliable prediction difficult [65, 66].

## 7 Advanced stages of thermonuclear burning

As the helium burning progresses, the stellar core is increasingly made up of C and O. At the end of helium burning, all hydrogen and helium is converted into a mixture<sup>18</sup> of C and O, and since H, He are most abundant elements in the original gas from which the star formed, the amount of C and O are far more in the core than the traces of heavy elements in the gas cloud. Between these two products, the Coulomb barrier for further thermonuclear reaction involving the products is lower for C nuclei. At first the C+O rich

---

tum  $l$  adds upto the angular momentum of the resonant state  $J = j_1 + j_2 + l$ . Therefore, for spin-less particles like the closed shell nuclei  $^4\text{He}, ^{16}\text{O}$  ( $j_1 = 0, j_2 = 0$ ), we have  $J = l$ . In the entrance channel of the reacting particles, the parity would be:  $(-1)^l \pi(j_1) \pi(j_2) = (-1)^{l=0} (1)(1)$ . If the parity of the resonance state were the same as that of the entrance channel, then the resultant state would have been a ‘‘natural parity’’ state. However, since the 4.97 MeV state in  $^{20}\text{Ne}$  has an assignment:  $J^\pi = 2^-$ , this is an ‘‘unnatural parity’’ state.

<sup>18</sup> Note however the caveat: if the amount of  $^{12}\text{C}$  is little (either due to a long stellar lifetime of He burning or due to a larger rate of the  $^{12}\text{C} + \alpha \rightarrow ^{16}\text{O} + \gamma$  reaction whose estimate outlined in the earlier section is somewhat uncertain), then the star may directly go from He-burning stage to the O-burning or Ne-burning stage skipping C-burning altogether ([67]).

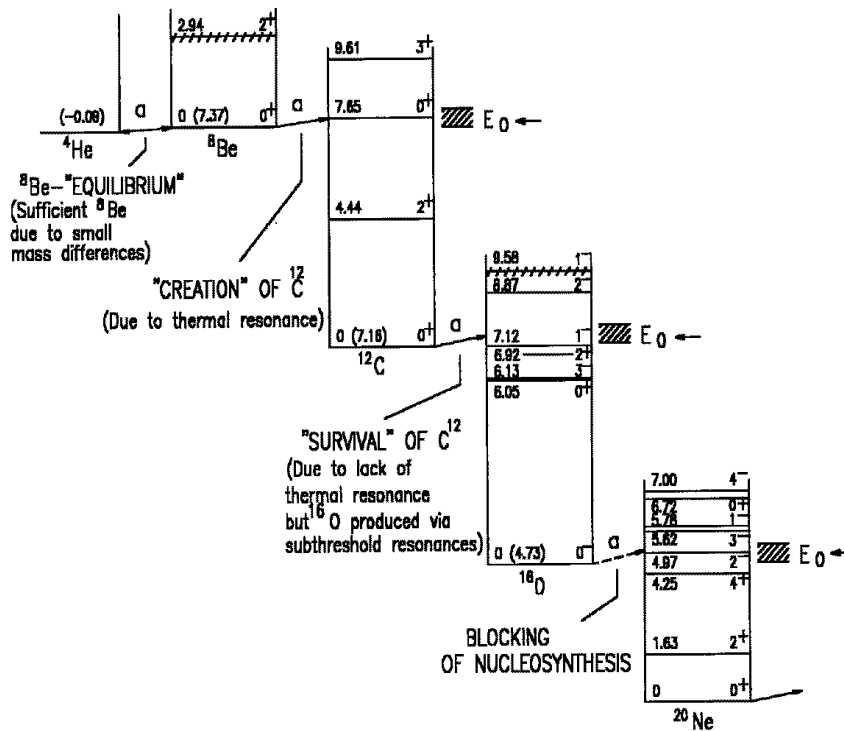


**Fig. 13.** Energy levels of nuclei participating in thermonuclear reactions during the helium burning stage in red giant stars (after [13]). Survival of both <sup>12</sup>C and <sup>16</sup>O in red giants, from which terrestrial abundances result, depends upon the fortuitous circumstances of nuclear level structures and other properties of these nuclei.

core is surrounded by He burning shells and a helium rich layer, which in turn may be surrounded by hydrogen burning shell and the unignited hydrogen rich envelope. When the helium burning ceases to provide sufficient power, the star begins to contract again under its own gravity and as implied by the Virial theorem the temperature of the helium exhausted core rises. The contraction continues until either the next nuclear fuel begins to burn at rapid enough rate or until electron degeneracy pressure halts the infall.

### 7.1 Carbon burning

Stars somewhat more massive than about 3 M<sub>⊙</sub> contract until the temperature is large enough for carbon to interact with itself (stars less massive on the main

sequence may settle as degenerate helium white dwarfs). For stars which are more massive than  $M \geq 8-10 M_{\odot}$  (mass on the main sequence, - *not* the mass of the C+O core), the contracting C+O core remains non-degenerate until C starts burning at  $T \sim 5 \times 10^8 K$  and  $\rho = 3 \times 10^6 \text{ gcm}^{-3}$ . Thereafter sufficient power is generated and the contraction stops and quiescent (hydrostatic, not explosive) C-burning proceeds (see Fig. 14).

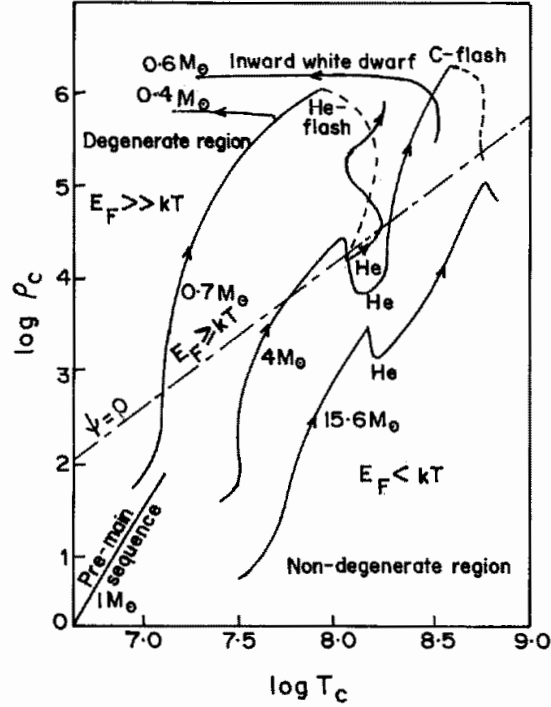
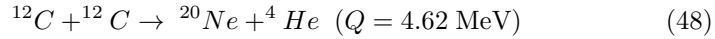


**Fig. 14.** Tracks in the core temperature, density plane of stars of various masses (at the start of hydrogen burning i.e. main sequence masses). Note that a star of mass  $M \sim 15M_{\odot}$  ignites all its fuels in non-degenerate conditions, whereas a star of mass  $M \sim 4M_{\odot}$  ignites carbon under strongly degenerate conditions. (After [68]).

The combined mass of two reacting  $^{12}\text{C}$  nuclei falls at an excitation energy of 14 MeV in the compound nucleus of  $^{24}\text{Mg}$ . At this energy there are many compound nuclear states, and the most effective range of stellar energies (the Gamow window) at the relevant temperature is about 1 MeV; hence a number of resonant states can contribute to the decay of the compound nucleus, and

even the large angular momentum resonances may be important because the penetration factors in massive nuclei are not affected by centrifugal barriers. The carbon on carbon burning can proceed through multiple, energetically allowed reaction channels, listed below:



At the temperatures where carbon burning starts, the neutron liberating reactions requires too much particle kinetic energy to be effective. In addition, based on laboratory measurements at higher energies compared to the stellar energies, the electromagnetic decay channel ( $^{24}\text{Mg} + \gamma$ ) and the three particle channel ( $^{16}\text{O} + 2\alpha$ ) have lower probability compared to the two particle channels:  $^{23}\text{Na} + p$  and  $^{20}\text{Ne} + \alpha$ . The latter two channels have nearly equal probabilities (see [14]; at the lowest center of mass energies for which cross-sections are measured in the laboratory for the proton and  $\alpha$  channels, (i.e. about 2.45 MeV [69]), the branching ratios were  $b_p \sim 0.6$  and  $b_\alpha \sim 0.4$ ), and therefore the direct products of carbon burning are likely to be  $^{23}\text{Na}$ ,  $^{20}\text{Ne}$ , protons and alpha particles. The rate for this reaction per pair of  $^{12}\text{C}$  nuclei is ([70]):

$$\log\lambda_{12,12} = \log f_{12,12} + 4.3 - \frac{36.55(1 + 0.1T_9)^{1/3}}{T_9^{1/3}} - \frac{2}{3}\log T_9 \quad (51)$$

the factor  $f_{12,12}$  is a screening factor. Now, at the temperatures of  $^{12}\text{C}$  burning, the liberated protons and alpha particles can be quickly consumed through the reaction chain:  $^{12}\text{C}(p, \gamma)^{13}\text{N}(e^+ \nu_e)^{13}\text{C}(\alpha, n)^{16}\text{O}$ . Thus, the net effect is that the free proton is converted into a free neutron (which may be further captured) and the  $\alpha$ -particle is consumed with  $^{12}\text{C}$  into  $^{16}\text{O}$ . The  $\alpha$ -particles are also captured by other alpha-particle nuclei, resulting in, at the end of carbon burning in nuclei like:  $^{16}\text{O}$ ,  $^{20}\text{Ne}$ ,  $^{24}\text{Mg}$  and  $^{28}\text{Si}$ . These secondary reactions augment the energy released by the initial carbon reaction and Reeves (1959) estimated that each pair of  $^{12}\text{C}$  nuclei release about 13 MeV of energy. Towards the end of carbon burning phase there are also other reactions such as:  $^{12}\text{C} + ^{16}\text{O}$  and  $^{12}\text{C} + ^{20}\text{Ne}$  which take place. But these are less rapid and are not expected to play major roles compared to the  $^{12}\text{C} + ^{12}\text{C}$  reactions, due to their increased Coulomb barriers. A recent discussion of the heavy ion reactions involving C and O is contained in [1] section 3.6.

During the carbon-burning and subsequent stages, the dominant energy loss from the star is due to neutrinos streaming out directly from the stellar thermonuclear furnace, rather than by photons from the surface. The neutrino luminosity is a sensitive function of core temperature and quickly outshines the

surface photon luminosity of the star at carbon burning stage. The (thermal) evolutionary time scale of the star, due to the neutrino emission becomes very short and the core evolves rapidly, – so rapidly (compared to the “cooling” time scale Kelvin-Helmholtz time:  $\tau_{KH} \sim GM^2/RL_{ph}$ ) that the conditions in the core are “uncommunicated” to the surface, since this happens by photon diffusion. The surface conditions (e.g. the temperature) then does not change much as the core goes beyond the carbon burning stage, and it may not be possible just by looking at a star’s surface conditions whether the core is close to a supernova stage or has many thousands of years of hydrostatic thermonuclear burning to go.

## 7.2 Neon burning

The result of carbon burning is mainly neon, sodium and magnesium, but aluminum and silicon are also produced in small quantities by the capture of  $\alpha$ ,  $p$  and  $n$  released during carbon burning. When carbon fuel is exhausted, again the core contracts and its temperature  $T_c$  goes up. At approximately  $T_9 \sim 1$ , energetic photons from the high energy tail of the Planck distribution function can begin to disintegrate the  $^{20}\text{Ne}$  ash (see Fig. 13) so that one has the reaction:  $^{20}\text{Ne} + \gamma \rightarrow ^{16}\text{O} + ^4\text{He}$ .

Nucleons in a nucleus are bound with typical binding energy of several to 8 MeV. An energetic  $\gamma$ -ray photon is required to photo-eject a nucleon. Two nucleon ejection requires more energy. Alpha particles are however released at approximately the same energy as a nucleon due to the low separation energy of an alpha particle in the nucleus. For example, the alpha separation energy in  $^{20}\text{Ne}$  is 4.73 MeV. Thus, the major photo-nuclear reactions are:  $(\gamma, n)$ ,  $(\gamma, p)$  and  $(\gamma, \alpha)$  processes. For a photo-disintegration reaction to proceed through an excited state  $E_X$  in the mother, the decay rate is:-

$$\lambda(\gamma, \alpha) = \left[ \exp\left(-\frac{E_X}{kT}\right) \frac{2J_R + 1}{2J_0 + 1} \frac{\Gamma_\gamma}{\Gamma} \right] \times \frac{\Gamma_\alpha}{\hbar} \quad (52)$$

In the above equation, the first factor in square brackets on the RHS is the probability of finding the nucleus in the excited state  $E_X$  and spin  $J_R$  (with  $J_0$  being the ground state spin), while the second factor  $\Gamma_\alpha/\hbar$  is the decay rate of the excited state with an alpha particle emission. Now since  $E_X = E_R + Q$ , we have:

$$\lambda(\gamma, \alpha) = \frac{\exp(-Q/kT)}{\hbar(2J_0 + 1)} (2J_R + 1) \frac{\Gamma_\alpha \Gamma_\gamma}{\Gamma} \exp(-E_R/kT) \quad (53)$$

At  $T_9 \geq 1$ , the photo-disintegration is dominated by the 5.63 MeV level in  $^{20}\text{Ne}$  (see Fig. 13). At approximately  $T_9 \sim 1.5$ , the photo-dissociation rate becomes greater than the rate for alpha capture on  $^{16}\text{O}$  to produce  $^{20}\text{Ne}$  (i.e. the reverse reaction), thus leading effectively to the net dissociation of  $^{20}\text{Ne}$ . The released  $^4\text{He}$  reacts with the unspent  $^{20}\text{Ne}$  and leads to:  $^4\text{He} + ^{20}\text{Ne} \rightarrow$

$^{24}\text{Mg} + \gamma$ . Thus the net result of the photo-dissociation of two  $^{20}\text{Ne}$  nuclei is:  $2 \times ^{20}\text{Ne} \rightarrow ^{16}\text{O} + ^{24}\text{Mg}$  with a net Q-value of 4.58 MeV. The brief neon burning phase concludes at  $T_9$  close to  $\sim 1.5$ .

### 7.3 Oxygen burning

At the end of the neon burning the core is left with a mixture of alpha particle nuclei:  $^{16}\text{O}$  and  $^{24}\text{Mg}$ . After this another core contraction phase ensues and the core heats up, until at  $T_9 \sim 2$ ,  $^{16}\text{O}$  begins to react with itself:



The first reaction takes place approximately 45% of the time with a Q-value of 9.593 MeV. In addition to Si and S, the oxygen burning phase also produces, Ar, Ca and trace amounts of Cl, K, etc upto Sc. Then at  $T_9 \sim 3$ , the produced  $^{28}\text{Si}$  begins to burn in what is known as the Si burning phase.

### 7.4 Silicon burning

As we have seen, most of the stages of stellar burning involve thermonuclear fusion of nuclei to produce higher Z and A nuclei. The first exception to this is neon burning where the photon field is sufficiently energetic to photo-dissociate neon, before the temperature rises sufficiently to allow fusion reactions among oxygen nuclei to overcome their Coulomb repulsion. Processing in the neon burning phase takes place with the addition of helium nuclei to the undissociated neon rather than overcoming the Coulomb barrier of two neon nuclei. This trend continues in the silicon burning phase. In general, a photo-disintegration channel becomes important when the temperature rises to the point that the Q-value, i.e. the energy difference between the fuel and the products is smaller than approximately  $30k_B T$  ([71]).

With typical Q-values for reactions among stable nuclei above silicon being 8-12 MeV, photo-disintegration of the nuclear products of neon and oxygen burning begins to play an important role once the temperature exceeds:  $T_9 \geq 3$ . Then nuclei with smaller binding energies are destroyed by photo-dissociation in favor of their more more tightly bound neighbors, and many nuclear reactions involving  $\alpha$ -particles, protons and neutrons interacting with all the nuclei in the mass range  $A = 28 - 65$  take place. In contrast to the previous burning stages where only a few nuclei underwent thermonuclear reactions upon themselves, here the nuclear reactions are primarily of a rearrangement type, in which a particle is photo-ejected from one nucleus and captured by another and a given fuel nucleus is linked to a product nucleus by a multitude of reaction chains and cycles and it is necessary to keep track of many more nuclei (and many reaction processes involving these) than for

previous burning stages. More and more stable nuclei form in a nuclear reaction network as the rearrangement proceeds. Since there exists a maximum in the binding energy per nucleon at the  ${}^{56}\text{Fe}$  nucleus, the rearrangements lead to nuclei in the vicinity of this nucleus (i.e. iron-group nuclei).

In the mass range  $A = 28 - 65$ , the levels in the compound nuclei that form during silicon burning are so dense that they overlap. Moreover, at the high temperatures that are involved ( $T_9 = 3 - 5$ ), the net reaction flux may be small compared to the large forward and backward reactions involving a particular nucleus and a quasi-equilibrium may ensue between groups of nuclei which are connected between separate groups by a few, slow, rate-limiting reactions (“bottlenecks”). However, as the available nuclear fuel(s) are consumed and thermal energy is removed due to escaping neutrinos, various nuclear reactions may no longer occur substantially rapidly (“freeze-out”). Thielemann and Arnett [72] found that for cores of massive stars in hydrostatic cases, the bottlenecks between quasi-equilibrium (QSE) groups coincided with  $Z=21$  nuclei whereas for lower mass stars, lower temperatures and  $Y_e$  and higher density this bridge involved neutron rich isotopes of Ca capturing protons. Hix and Thielemann [71] discussed and contrasted these results with those of earlier workers; in general the reaction flow across the boundary of the QSE groups are influenced by the neutronization of the material, i.e. the overall  $Y_e$ . It is in this context that weak interaction processes such as electron capture and beta decay of nuclei are important, by influencing the  $Y_e$  and thereby the reaction flow. These ultimately affect both the stellar core density and entropy structures, and it is important to track and include the changing  $Y_e$  of the core material not only in the silicon burning phase, but even from earlier oxygen burning phases. The calculation of stellar weak processes on nuclei has spawned extensive literature (see [73], [74], [75] etc., and for a review [76]).

Iron, nickel and neighboring nuclei which are the products of the hydrostatic Si burning in the core are mostly trapped in the collapsing core that ends up as the compact remnant and little of this may reach the interstellar medium. However, the blast wave shock launched after the core bounce impacts through the onion-like outer shells that the star’s earlier evolution has left behind. The nearest part of the Si shell that is still unburned is heated to sufficient temperatures to form iron peak nuclei. Regions which are not as close can undergo incomplete Si burning and be left with substantial amounts of Si, S, Ar, Ca and Ti. Three separate outcomes may result depending upon the initial density and the peak temperature: 1) incomplete Si burning; 2) a “normal freezeout” and 3) an “ $\alpha$ -rich freezeout”. In the first case, with initial temperatures of about  $5 \times 10^9\text{K}$  and peak density of  $\rho = 10^9 \text{ g cm}^{-3}$ , significant amounts of Si and other intermediate-mass elements remain after the charged particle reactions freezeout in the expanding ejecta. In the normal freezeout, an initial condition of  $7 \times 10^9\text{K}$  and peak density of  $\rho = 10^9 \text{ g cm}^{-3}$  leads to complete Si burning. The “ $\alpha$ -rich freezeout” however takes place at lower peak densities  $\rho = 10^7 \text{ g cm}^{-3}$  though similar peak temperatures:  $7 \times 10^9\text{K}$ . This ends up with an abundance of  ${}^4\text{He}$  nuclei which produces a significant flow

through the triple alpha reaction into intermediate mass nuclei, in addition to the iron group nuclei products. The feedback between the rate of nuclear recombination and that of temperature evolution in the expansion critically controls the “ $\alpha$ -richness” of matter and production of important radioactive nuclei e.g.  $^{44}\text{Ti}$  and is one of the challenges of computational simulation of silicon burning. For a recent discussion of the computational aspects of the nuclear evolution during silicon burning, see [77].

In summary, a few key points concerning the thermonuclear burning of  $^{28}\text{Si}$  are as follows:-

- Direct thermonuclear fusion of two  $^{28}\text{Si}$  nuclei does not take place because their Coulomb barrier is too high. Instead thermonuclear fusion takes place by successive additions of  $\alpha$ -particles, neutrons and protons.
- Although this is actually a large network of nuclear reactions it is called “silicon burning” because  $^{28}\text{Si}$  offers the largest resistance to photo-dissociation because of its highest binding energy among intermediate mass nuclei.
- The source of the  $\alpha$ -particles which are captured by  $^{28}\text{Si}$  and higher nuclei is  $^{28}\text{Si}$  itself. Silicon, sulphur etc. partially melt-down into  $\alpha$ -particles, neutrons and protons by photo-dissociation. These then participate in reaction networks involving quasi-equilibrium clusters linked by “bottleneck” links.
- Although beta decay and electron captures on stellar core nuclei do not produce energy in major ways they nevertheless play a crucial role in shifting the pathways of nuclear and thermodynamic evolution in the core conditions. These ultimately determine the mass of the core and its entropy structure which finally collapses in a supernova explosion.

## 8 Core collapse SNe: electron capture and neutrinos

At the end of nuclear burning in the core of a massive star, inert Iron group nuclei are left in the innermost region, – inert because nuclear burning cannot extract any further energy from the most tightly bound nuclei. At the last stages of nuclear burning, neutrino cooling which is far more efficient than the radiation of photons from the surface, would leave the core compact and degenerate [78] (where electron Fermi energy is much larger than the thermal energy  $kT$ ) due to a number of processes such as  $e^+/e^-$  pair annihilation process, photoneutrino process and plasmon decay into neutrinos. These neutrinos escape from the star freely at this stage since their interaction cross section is so small, much smaller than that of the photons. In the picture of the late stages of a spherical star that B<sup>2</sup>FH [79] proposed one had an onion-skin model: nested shells of progressively heavier elements, with the densest iron core at the center. Successively high-Z elements are ignited in increasingly central parts of the core in decreasingly lower specific entropy environments, and are contained within entropy barriers left behind by previous generations of nuclear burning. The degenerate core becomes unstable

to gravitational collapse at roughly the same Chandrasekhar mass (modulo relatively small variations in the electron fraction or entropy profiles in the core) practically independent of the total mass of the star, which for example could range from  $\sim 8M_{\odot}$  to  $\sim 60M_{\odot}$  [67]. This “core convergence” establishes the important connection between the Chandrasekhar mass and the masses of neutron stars that are formed from core-collapse supernovae (though the details of the boundaries of the main sequence masses that lead to neutron stars, as well as the composition of the cores, e.g. O-Mg-Ne cores vs iron cores etc., have evolved as further research was undertaken). The supernova explosion itself is triggered by the collapse of the core [80], followed by the sudden release of gravitational energy. When the iron core grows in size, its temperature increases, and when  $T > 7 \times 10^9 K$ , iron nuclei photo-dissociate in endothermic reactions (consuming energy, even though the free energy  $F = U - TS$  decreases due to increased entropy) into alphas and neutrons. This leads to the effective adiabatic index decrease below  $4/3$  and the iron core becomes unstable to collapse. Collapse initiation through photo-dissociation happens in relatively massive cores of more massive stars whereas in less massive stars the collapse may initiate due to reduction of electrons (which provide the bulk of the supporting pressure due to their high Fermi momenta) as they are captured by nuclei in “inverse beta decay” in regions where the electron Fermi energy exceed the capture thresholds.

The core collapses on a dynamical scale until the infall is suddenly halted when the central density overshoots that of the nuclear matter, at  $4 - 5 \times 10^{14} \text{gm cm}^{-3}$ . In between, the iron core collapsed onto itself nearly freely at about a quarter of the speed of light. Initially it had the size of the Earth, but towards the end it is a hot, dense, neutron rich sphere about 30 km in radius (see [81] for a review). A static accretion shock wave forms initially at the edge of the quasi-free falling core, which soon starts propagating outward through the outer core and mantle as more kinetic energy is brought into it by infalling matter. The shock wave soon stalls (at least for most of the range of main sequence masses beyond about  $10 M_{\odot}$ ) which may however be helped after about 500 milliseconds (“after a pause that refreshes” – according to Hans Bethe) [82] by neutrinos which are freely streaming out from the inner core, but manage to deposit enough energy (albeit a small fraction of their total energy) “reviving” the shock. During this post-bounce phase the proto-neutron star radiates away most of its energy ( $3 \times 10^{53}$  erg) in the form of neutrinos and antineutrinos of various flavors and this accounts for the larger intrinsic energy per unit mass of the central engines of core collapse SNe.

### 8.1 Electron capture on nuclei and protons: a core thermometer

During the gravitational collapse, the entropy of the core stays low, which permit the nuclei of various elements present in the core to (largely) survive thermal disintegration and coexist with a small fraction of “dripped” nucleons ([83] hereafter BBAL). Around the density  $5 \times 10^{11} \text{gm cm}^{-3}$ , neu-

trinos produced through electron capture on these nuclei and free protons are trapped in the core. Much of the information pertaining to the conditions in which the neutrinos are originally produced, such as the nuclear and thermodynamic properties of the core of the supernova are altered because these neutrinos undergo *inelastic* scattering with the overlying stellar matter in the post neutrino trapping phase. Neutrinos which are emitted through electron captures on the nuclei present in the pre-supernova and collapsing core *before* it reaches neutrino trapping density ( $\simeq 10^{12} \text{ gm cm}^{-3}$ ) [84], [85], however, stream freely through the stellar matter without any further interactions. These pre-trapping neutrinos carry with them information on both physical conditions within the core, as well as its nuclear configuration e.g. the ratio of the number density of free protons to that of heavy nuclei. The last quantity can depend on the nuclear equation of state relevant to collapse. Since neutrinos act as probes of the dynamic, thermodynamic and nuclear properties of the pre-supernova and collapsing core, their detection and measurement of energy spectrum can have significant implications. The time evolution of the detected spectrum could also reveal the dynamical time scale – a clue to the average density and mass of the stellar core which may have implications for neutron star vs black hole formation<sup>19</sup>. The reduction of lepton fraction during stellar collapse has implications for shock formation stages and the overall dynamics - even in the delayed explosion stage, since it determines, through the original energy of the bounce shock, and the entropy profile in the outer core, the position of the stalled shock.

The loss of neutrinos at low and intermediate densities is important in determining the saturation ratio of the lepton to baryon ratio at the time of core bounce (the leptons determine the pressure in the core whereas the baryons, mainly nucleons, determine the mass of the homologous collapsing core). Brown et al [87] argued that the hydrodynamic collapse is nearly homologous, i.e. the density structure of the collapsing core remains self-similar throughout the collapse until the time of bounce. This greatly simplifies the study of various processes during the collapse and quantities in the core can be calculated (largely semi-analytically) through the evolution of a “mean” “one-zone” symbolizing the core properties (see e.g. [88], [89]).

The core of a massive star collapses under its own gravity when the pressure support from degenerate electrons is reduced through the capture of electrons in the stellar material. The electron capture on neutron rich heavy nuclei initially proceeds primarily through the allowed type ( $\Delta l = 0$ ) Gamow Teller transitions. As core density exceeds  $\simeq 10^{11} \text{ gm/cm}^3$ , the nuclei become more and more massive and too neutron rich to allow  $e^-$ -capture to take place through allowed Gamow-Teller transitions from the ground state. This is because the allowed states for  $p$  to  $n$  transition within the nucleus are already filled by the neutrons (neutrons shell blocked) and the transition strength for typical captures like  $^{56}\text{Fe} \rightarrow ^{56}\text{Mn}$  used earlier (as in [90])

---

<sup>19</sup> The collapse of a star could in principle also lead to a “naked singularity” [86]

is no longer representative of typical nuclear  $e^-$ -capture rates. It was shown [91],[92] that the dominant unique first forbidden transition strength was actually negligible compared to the thermally unblocked strength under the typical core collapse conditions. Therefore, after neutron-shell blocking sets in, (when  $(A,Z) > {}^{74}\text{Ge}$ ) the sum rule for the Gamow Teller transition operator  $|M_{GT}|^2$  decreases from a typical value of 2.5 [90], [88] to about 0.1. The  $e^-$ -capture rate on a single nucleus  $X(A, Z)$  in the initial state  $i$  to the final state  $j$  is:

$$\lambda_{ij} = \ln 2 \frac{f_i(T, \mu_e, Q_{ij})}{ft_{ij}} \quad (56)$$

where  $ft_{ij}$  is related to  $|M_{GT}|^2$  by  $ft_{ij} = 3.596 - \log |M_{GT}|^2$  for allowed Gamow-Teller type transitions (for free protons,  $\log ft_{f.p.} = 3.035$ ). The factor  $f_i(T, \mu_e, Q_{ij})$  is the phase space factor for allowed transition, which is a function of the ambient temperature  $T$ , the Fermi-energy of the electron  $\mu_e$  and the Q-value for the reaction. The neutrino energy is  $E_{\nu_e} = E_e - Q_{ij}$ .

The change in entropy during collapse controls the fraction of the dripped protons with respect to that of the heavy nuclei and this influences the overall neutrino spectrum received on earth as the spectrum of neutrinos generated by electron capture on protons are different from captures on heavy nuclei. The received neutrino spectrum depends not only upon the initial conditions from which the collapse started, but also on the details of the electron capture properties of the stellar matter. Properties of nuclei at finite temperatures and density during this phase of the collapse, where shell and pairing corrections are relevant were computed in [94] and utilized to evolve self-consistently with the electron capture physics and the consequent changes in nuclear and thermodynamic variables.

The rate of generation of neutrinos per nucleon within energy band  $E_\nu$  to  $E_\nu + dE_\nu$  after accounting for the relative abundance of free protons and nuclei, is:

$$dY_\nu(E_\nu) = d\lambda_{fp}(E_\nu)X_p + d\lambda_H(E_\nu)(1 - X_n - X_p)/A \quad (57)$$

here  $A$  represents the Atomic weight of the ensemble of nuclei present in the core, taken to be represented by a single "mean" nucleus as in [90]. The differential neutrino production rates for free protons and heavy nuclei are:

$$d\lambda_{fp,H} = \frac{\log 2}{(ft)_{fp,H}} \frac{\langle G \rangle}{(m_e c^2)^5} \frac{E_\nu^2 (E_\nu + Q_{fp,H}) \sqrt{(E_\nu + Q_{fp,H})^2 - (m_e c^2)^2}}{(1 + \exp(E_\nu + Q_{fp,H} - \mu_e))} dE_\nu \quad (58)$$

where the Coulomb correction factor  $\langle G \rangle$  has been taken as  $\approx 2$  for heavy nuclei and 1 for free protons. The Q-value is given as:  $Q = (\hat{\mu} + 1.297 + E_{GT})$  assuming that the strength is concentrated in a single state and here  $\hat{\mu} (= \mu_n - \mu_p)$  is the difference in the neutron and proton chemical potentials when free nucleons coexist with a distribution of neutron rich nuclei in nuclear statistical

equilibrium, and  $E_{GT}$  is the energy of the Gamow-Teller Resonance centroid. The centroids in fp-shell nuclei, found from experimental data from (n,p) reactions have been used for characterizing GT transitions in these nuclei [93] and are close to the value (3 MeV) used here. The GT centroid in the e-capture direction is itself a function of the ambient temperatures as a quasi-particle random phase approximation (QRPA) calculation shows [95]. At the relevant high densities, when neutron rich nuclei with  $A > 65$ , are abundant and the electron chemical potential is noticeably larger than typical nuclear Q-values, electron capture rates are mainly sensitive to the centroid and total strength of the GT+ distributions – these are reasonably well described within the random phase approximation [96]. We note that the temperature dependence of the nuclear symmetry energy can also affect the neutronization of the stellar core prior to neutrino trapping during gravitational collapse [97], [98] since ambient temperatures can reach upto several MeV. Not only the reaction Q-values but also the equation of state of bulk dense matter, the free nucleon abundances, the degree of dissociation into alpha-particles and the nuclear internal excitations are modified by changes in the symmetry energy.

The Fermi-energy  $\mu_e = 11.1(\rho_{10}Y_e)^{1/3}\text{MeV}$ . The difference in chemical potentials  $\hat{\mu}$ , and the relative fraction of free protons are obtained from a low density analytic equation of state similar to that in [90] with modifications noted in [88]. Shown in Fig. 15 is a typical “snapshot” spectrum of neutrinos from a  $15 M_\odot$  star’s core collapse within a narrow range of stellar core density around  $10^{11} \text{ gm cm}^{-3}$ . Note the two separate peaks from captures on free protons and heavy nuclei which have non-thermal spectra.

## 8.2 Number of neutrinos emitted and predictions of detections

The number of neutrinos and their energy distributions that could have been detected by large underground neutrino experiments like the SuperKamioka experiment and the Sudbury Neutrino Observatory (SNO)<sup>20</sup> has been calculated [99]. The spectrally integrated fluence of  $\nu_e$  at a distance of 1 kpc, as  $Y_e$  changes from 0.42 to 0.39 in a  $1.4 M_\odot$  stellar core (of a  $15 M_\odot$  star) is:  $F_\nu = 4.2 \times 10^{11} \text{ cm}^{-2}$ . The energy of the infall neutrino burst up to this stage is:  $E_{\nu_e} = 7.2 \times 10^{50} \text{ erg}$ . The flux, direction and the spectra of the neutrinos could have been measured by the charge current dissociation of the deuterium nucleus ( $\nu_e(d, pp)e^-$ ) in the (“classic”) Sudbury Neutrino Observatory (SNO) [100] with a fiducial mass of 1 Kt of high purity  $\text{D}_2\text{O}$ . It would have been also possible to detect  $\nu_e$  and obtain spectral information by means of the

<sup>20</sup> The original SNO experiment with heavy water has finished taking data. Thus the heavy water based predictions if a nearby supernova took place are only indicative. However there are plans of an extended SNO (called SNO+) which will use 1 kTon of liquid scintillator which will greatly reduce the lower energy threshold of neutrinos and will remain sensitive to neutrinos from a nearby SN. Moreover, after an accident the photomultiplier tubes in SuperKamioka, the low energy thresholds originally designed for are no longer operative.

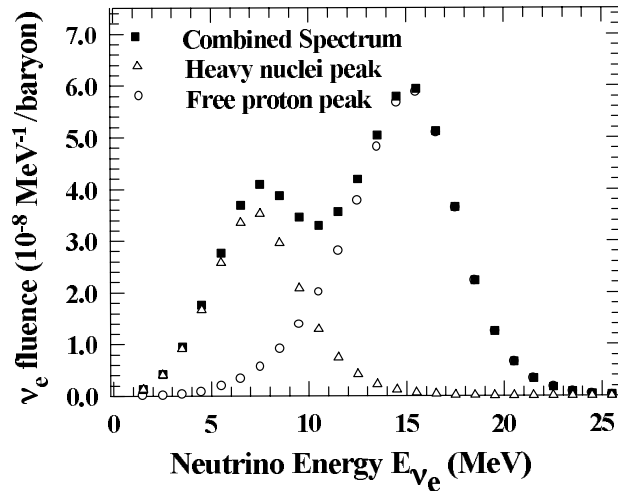


**Fig. 15.** “Snapshot” neutrino fluence ( $\text{MeV}^{-1} \text{baryon}^{-1}$ ) in a density interval  $\Delta\rho_{10} = 0.0002$  around  $\rho_{10} = 9.8668 \text{ gm cm}^{-3}$  for a  $15 M_{\odot}$  star ( $D = 1 \text{ kpc}$ ) [99].

neutrino-electron scattering reaction ( $\nu_e + e^- \rightarrow \nu_e + e^-$ ) in SNO as well as in the light water detector Super Kamioka. Apart from the reactions mentioned above which can perform spectroscopy (i.e. measure the incoming neutrino energy), the neutral current dissociation of  $d$  by the reaction  $\nu_e(d, pn)\nu_e$  could have obtained the the total neutrino flux (of all flavors). The number of  $\nu_e$  events which could have been detected in the SNO detector through neutrino-induced c.c. reaction on the target  $d$  nuclei is given by:  $n_{\nu_e} = F_{\nu} \sigma_{cc}(\epsilon_{\nu_e}) N_d$  where  $N_d (= 6.02 \times 10^{31})$  is the total number of target nuclei present in the 1Kt detector. The charge current and neutral current cross-sections ( $\sigma_{cc}(\epsilon_{\nu_e})$  and  $\sigma_{nc}(\epsilon_{\nu_e})$  respectively), have been computed for the  $\nu$ - $d$  process by Bahcall et al. [101] and accurate fits to these cross-sections between 5 to 40 MeV are given as [102]:  $\sigma_i = \alpha_i (\epsilon_{\nu} - \epsilon_{th,i})^{2.3}$  where  $i = cc$  and  $nc$ ,  $\alpha_{cc} = 1.7 \times 10^{-44} \text{ cm}^2$ ,  $\alpha_{nc} = 0.85 \times 10^{-44} \text{ cm}^2$ ,  $\epsilon_{th,cc} = 2.2 \text{ MeV}$  and  $\epsilon_{th,nc} = 1.44 \text{ MeV}$ .

For the  $\text{H}_2\text{O}$  based Cerenkov detector (Super-Kamioka) the  $(\nu_e, e^-)$  scattering events would be the main source of  $\nu_e$  spectral information since the corresponding energy thresholds for charge current and neutral current interactions for ordinary water are much higher. (During the collapse stage, the neutrino flux is almost entirely in neutrinos of the electron type; anti-neutrinos of various kinds, as well as neutrinos of the mu or tau type are generated in copious numbers only in the hot post core bounce phase). The relevant  $(\nu_e, e^-)$  scattering cross-section is [103]:  $\sigma_e = (1/2)(4G^2 m_e^2 \hbar^2 / \pi c^2)(7/12)(\epsilon_{\nu} / m_e c^2)$ .

The number of detections by Super-Kamioka (mass 32 kt) and SNO for a supernova explosion 1 kpc away, for several possible scenarios of stellar core collapse are reported in Table 2 [99]. The  $15 M_{\odot}$  star collapse is initiated from thermodynamic conditions as in [88] ( $Y_{ei} = 0.420$ ,  $S_i/k_B = 1.00$ ,  $T_i = 0.7178$ ,  $\rho_{10} = 0.37$ ), while the  $25 M_{\odot}$  star's single zone initial conditions are similarly derived from the data reported in [104] and an expression for the core averaged entropy ( $Y_{ei} = 0.423$ ,  $S_i/k_B = 1.14$ ,  $T_i = 0.6756$ ,  $\rho_{10} = 0.15$ ).

**Table 2.** Pre-trapping neutrino detections predicted in SNO (heavy water) and Super Kamioka [99] with hardness ratios up to  $\rho_{10} = 24.16$  for indicated heavy nuclear e-capture matrix elements for  $15 M_{\odot}$  Fuller (1982) and  $25 M_{\odot}$  WWF presupernova stars. Note the caveat in footnote 20.

| Star Mass      | $ M_{GT} ^2$ | $t_{collapse}$<br>(ms) | Pre-trapping Variables |           | No. Detected |     | Hardness Ratio <sup>†</sup> |        |
|----------------|--------------|------------------------|------------------------|-----------|--------------|-----|-----------------------------|--------|
|                |              |                        | $Y_{ef}$               | $S_f/k_B$ | SNO          | S-K | SNO                         | S-K    |
| $15 M_{\odot}$ | 1.2/0.1      | 120                    | 0.3909                 | 1.0021    | 82           | 394 | 0.2786                      | 0.8540 |
|                | 2.5/0.1      | 120                    | 0.3896                 | 1.0085    | 66           | 344 | 0.2876                      | 0.9537 |
| $25 M_{\odot}$ | 1.2/0.1      | 190                    | 0.3828                 | 1.1080    | 120          | 566 | 0.2878                      | 0.8319 |
|                | 2.5/0.1      | 190                    | 0.3813                 | 1.1204    | 99           | 499 | 0.2916                      | 0.9190 |

<sup>†</sup> The hardness ratio denotes the number of neutrino events in the  $5 \text{ MeV} \leq E_{\nu_e} \leq 12 \text{ MeV}$  and  $12 \text{ MeV} \leq E_{\nu_e} \leq 25 \text{ MeV}$  bands.

Neutrino spectroscopy of the final state of a star would be possible provided that the event occurs at a relatively close distance. Although, a priori, these may be rare events, there have been a number of historical Supernovae, as well as detected radio pulsars within a distance of about 2 kpc. There are a number of star forming regions nearby (such as the Orion complex - about 440 pc away), which are sites of potential supernova progenitor. A detection by underground neutrino experiments would constrain features of theoretical calculations of both collapse and explosion era of type II Supernovae as well as shed light on the characteristics of the stellar core. The 19 neutrinos detected from SN1987A were most likely to have been emitted during the post-bounce phase as their total fluence during the proto neutron star cooling phase (at  $\simeq 10^{58}$ ) is much larger than that during the collapse phase ( $\simeq 10^{56}$ ).

## 9 Detected neutrinos from SN 1987A and future neutrino watch

Gravitational collapse of the core of the massive star under its own gravity leads to a supernova explosion. These are extremely energetic explosions where the observable energy in the kinetic energy of the exploded debris and electromagnetic radiation add up to several times  $10^{51}$  erg. The actual energy

scale is typically  $3 \times 10^{53}$  erg or higher, but most of this is radiated away neutrinos. Although the full understanding of the process of explosion in a gravitational collapse leading to a supernova has not been achieved despite several decades of theoretical and computational work, a watershed in the field was achieved observationally when a supernova exploded close by in a satellite galaxy of our own, namely SN1987A in the Large Magellanic Cloud (LMC). A few neutrinos were detected from this supernova [105], [106], which were the first detections of the astrophysical neutrinos from outside of our solar system. By using the energetics of the neutrinos, their approximate spectral distribution, the distance to the LMC it was possible to show that the overall energy of the explosion was indeed  $E_T \sim 2 - 3 \times 10^{53}$  erg.

In addition, the duration of the neutrino burst was of the order of a few seconds as opposed to a few milliseconds, signifying that the observed neutrinos had to diffuse out of the dense and opaque stellar matter as predicted theoretically, instead of directly streaming out of the core. The spectral characteristics also indicated that the object that is radiating the neutrinos was indeed very compact, roughly of the same dimensions as that of a protoneutron star. Thus SN1987A provided the observational confirmation of the broad aspects of the theoretical investigation of stellar collapse and explosion. For a review of the understanding of the astrophysics of SN1987A, see [107].

Physicists are now gearing up to detect not only another supernova in our own galaxy, but by hoping to build very large neutrino detectors, they aim to detect supernova neutrinos from the local group of galaxies ([108], [109]). As neutrinos from the supernova travel directly out from the core, they arrive a few hours ahead of the light flash from the exploding star, since light can only be radiated from the surface of the star, and it takes the supernova shock launched at the deep core several hours to reach the surface. In the case of SN1987A, this time delay allowed the estimation of the size of the star that exploded. Thus some advance warning of the supernova in the optical band can be gotten from a “neutrino watch”. Physicists have now connected a worldwide array of neutrino detectors through the Internet (SN Early Warning System or SNEWS<sup>21</sup>) which will notify astronomers to turn their optical, UV and other telescopes to the right direction when they find a burst of neutrinos characteristic of a supernova explosion.

## 10 What X-ray spectroscopy reveals about nucleosynthesis in SNe and SNRs

X-rays from a supernova explosion arise from the interaction of the supersonic ejecta with the circumstellar medium (CSM). The CSM typically consists of a slow-moving wind. When the ejecta collides with the CSM, it creates two shocks: a high-temperature, low-density, forward-shock ploughing through

---

<sup>21</sup> See the site: <http://hep.bu.edu/~snnet/>

the CSM (known as blast-wave shock) and a low-temperature, high-density, reverse-shock moving into the expanding ejecta. Initially the X-rays come from the forward-shocked shell dominated by continuum radiation, but after a few days X-rays arise also from the reverse-shock, which can have substantial line emission, thus providing nucleosynthetic fingerprints of the ejecta. The temporal evolution of the X-ray luminosity of a supernova can yield information on the density distribution in the outer parts of the exploding star ( $\rho \propto r^{-n}$ , here  $n$  can be in the range 7 – 12, typically  $n \sim 10$  for a Blue Supergiant (BSG) and  $n \sim 12$  for a Red Supergiant (RSG)- see [110]). These studies are therefore of interest to stellar structure and evolution.

To date thirty-six supernovae have been detected in the X-ray bands<sup>22</sup>. Among these the most extensively studied is SN 1987A because it was so bright. Another extensively studied object, of the supernova remnant (SNR) kind is Cassiopeia A. A SNR is just an older supernova after it has picked up enough material from the surrounding medium, which slows it down. The debris of the explosion, or the ejecta, radiates when it is reheated after an initial cooling, having been hit by a inward propagating reverse shock.

### 10.1 Supernova Remnant Cassiopeia A

Cassiopeia A (Cas A for short and also known as 3C461 or G111.7-2.1) is the second youngest SNR in our Milky Way galaxy. It was believed to be the product of a SN explosion in  $\sim 1672$  [112] only about 3.4 kpc away [113]. The British astronomer John Flamsteed may have recorded it as a sixth magnitude star in 1680, but it may have faded rapidly after explosion which could have acted against its widespread reportage. It is a shell type SNR which was rediscovered by radio astronomers Ryle and Smith [114] and is the brightest extra-solar radio object. Cas A is an oxygen-rich SNR with heavy element distribution typical of a core-collapse SN. Its closeness, young age and high brightness across the whole electromagnetic spectrum have underscored its importance for studying supernovae<sup>23</sup>. A recent optical spectrum of the original supernova near maximum brightness, obtained from scattered light echo more than three centuries after the direct light of the explosion was received on Earth, showed it to be a type IIb SN [116]<sup>24</sup>, somewhat like the well studied

<sup>22</sup> See S. Immler's X-ray supernova page at [http://lheawww.gsfc.nasa.gov/users/immler/supernovae\\_list.html](http://lheawww.gsfc.nasa.gov/users/immler/supernovae_list.html) and [111].

<sup>23</sup> Here we discuss thermal emission from Cas A, which directly connects to nucleosynthetic products. Many shell-type SNRs, including Cas A, also show non-thermal synchrotron X-rays - see [115].

<sup>24</sup> Krause et al note that even with the overall lack of hydrogen emission in most knots and the nitrogen enrichment in the remnant which is widely interpreted as signatures of the collapse of a Wolf-Rayet star, i.e. a type Ib SN [117], Cas A cannot be classified as arising out of a type Ib SN, since Cas A light echo spectrum does not match well the spectrum of the prototype SN 2005bf.

prototype SN 1993J<sup>25</sup> [123]. The estimated mass loss rate of  $2 \times 10^{-5} M_{\odot} \text{ yr}^{-1}$  and a wind velocity of  $10 \text{ km s}^{-1}$  consistent with the hydrodynamical state of the Cas A remnant [124] is also similar to what has been interpreted from radio and X-ray observations of SN 1993J [125],[126].

SNR Cassiopeia A has a bright clumpy emission ring with a diameter of about  $3'$ . This is associated with the SNR ejecta, whereas at an outer diameter of about  $5'$ , there is fainter emission in a filamentary ring which is due to the forward (“blast-wave”) shock in the circumstellar medium. The SNR has a nearly circular appearance, though the ejecta shows a bipolar structure, and jets (mainly in the NE, i.e. upper left of the image and a fainter extension in the SW direction, called the “counterjet”) that were formed by the explosion (detected both in the optical [127] and in the Si line X-ray emission [129], [128]). The remnant has been extensively observed in the optical and more recently with a million second exposure of the Chandra X-ray Observatory [128] (see also XMM-Newton [130]) and includes high resolution grating X-ray spectroscopy with Chandra [131] as also the Spitzer Space Telescope using the Infrared Array Camera [132] and the IR Spectrograph [133].

Many of Cas A’s optically bright knots have been identified as shocked ejecta which is still visible due to its young age. The optical radiation emitting regions have been classified into two groups: the so called fast moving knots (or ‘FMK’s with speeds  $4000 \text{ km s}^{-1} < v < 15000 \text{ km s}^{-1}$ ) and the slow moving quasi-stationary foci (or ‘QSF’s with speeds  $v < 300 \text{ km s}^{-1}$ ). The FMKs believed to comprise of SN ejecta, have H-deficient emission (lacks in  $H\alpha$ ) which is dominated by forbidden lines of O and S emission [134] while the QSF emission is rich in N, and is believed to originate from the gas lost from the star before its explosion (circumstellar envelope) which is now hit by the blast wave shock [131].

Cas A shows the nucleosynthesis products of both hydrostatic and explosive nucleosynthesis. C and O are produced in He burning, Ne and Mg first appears through C burning, and O and Al are added with Ne burning [135]. Spectral lines of heavier elements: Si, S, Ar, Ca etc are seen. These are produced in O burning, with alpha reactions on Mg also contributing, – they are from zones where explosive O-burning and incomplete explosive Si-burning occurs. Fe group elements are produced in the “Si burning” chain of reactions and result from complete and incomplete Si-burning. Much of the layered

---

<sup>25</sup> The collapse of a red supergiant [118] in a binary system [119] with the larger star with a mass on the main sequence of  $\sim 10$  to  $20$  led to SN 1993J and could explain its light curve and other characteristics [120], [121]. Photometry and spectroscopy at the position of the fading SN with Hubble Space Telescope and Keck Telescope, a decade after its explosion showed the signature of a massive star, – the companion to the progenitor that exploded. While the binary system initially consisted of e.g. a  $15M_{\odot}$  star and  $14M_{\odot}$  star in an orbit of 5.8 yr, at the time of the explosion, the primary had a mass of  $5.4M_{\odot}$  (with a helium exhausted core of  $5.1M_{\odot}$ ) and a secondary which gained mass in transfer and which we still see today, ended up with  $22M_{\odot}$  [122].

nucleosynthetic structure has been preserved during the explosion process in Cas A, with layers of N-, S-, O-rich ejecta seen beyond the outer shock [134]. However, in the optical bands, “mixed emission knots” showing N and S lines suggest that clumps of high speed S ejecta have penetrated through outer N-rich layers [134]. X-ray line data show that for example, in the southeast region of the SNR, Fe is farther out and is moving faster than the Si/O region. Hughes et al [136] consider the high surface brightness knots enriched in Si and S are consistent with nucleosynthetic products of explosive O burning, whereas elsewhere, the more diffuse, lower surface brightness features with enhanced Fe could be the result of explosive Si burning.

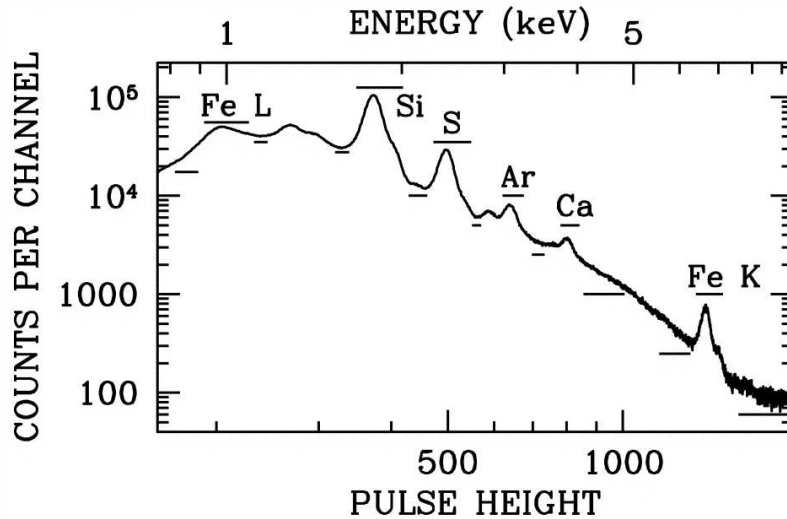


**Fig. 16.** Spectrum of the entire supernova remnant Cassiopeia A taken by Chandra (AXAF CCD Imaging Spectrometer (ACIS)) on January 30-31, 2000 against pulse height (lower x-axis) in the spectral channel and photon energy (upper x-axis) using a gain value of 4.8 eV per channel (Fig. reproduced by permission of the AAS and courtesy of U. Hwang [129]).

The “non-dispersed”<sup>26</sup> X-ray CCD spectrum for the entire Cas A remnant is shown in Fig. 16. A 50 ks exposure in January 2000 collected approximately 16 million photons during the observation of the SNR. It shows prominent lines of Si, S, Ar, and Ca, in their Helium-like ionic state and undergoing ( $n = 2 \rightarrow n = 1$ ) transitions as also the L and K transitions of Fe.

Maps were constructed of the entire remnant in the spectral line energies of several specific elements. The Si and S X-ray line maps and the optical

<sup>26</sup> This means the X-ray beam did not pass through any dispersive element like a grating, but the spectrum is obtained by measuring the energy of the incident X-ray by the intrinsic spectral sensitivity of the CCD.

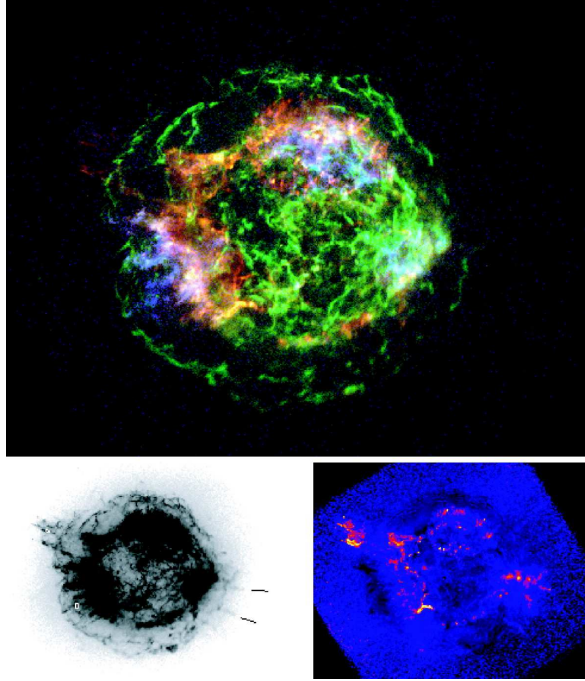


**Fig. 17.** Top: Three-color image of Cas A with red = Si He $\alpha$  (1.782.0 keV), blue = Fe K (6.526.95 keV), and green = 4.26.4 keV continuum. The remnant is roughly 5' across. Bottom left: Overexposed broadband image showing faint features. The spectral regions are indicated (top left of this box: northeast jet; bottom left of this box: Fe-rich region; lines at bottom right point to two southwest jet filaments). Bottom right: On the same scale, the ratio image of the Si He $\alpha$  (1.782.0 keV) and 1.31.6 keV (Mg He $\alpha$ , Fe L), without subtraction of the continuum contribution. The image highlights the jet and counterjet traced by Si emission, although features at the lowest intensity levels are uncertain. (Figure reproduced by permission of the AAS and courtesy of U. Hwang [128]).

maps resemble each other and this demonstrated that the X-ray and optically emitting ejecta are largely spatially coexistent. In fact the X-ray Si and S line emission, expected to include a significant contribution from the ejecta, shows asymmetric Doppler shifts corresponding to bulk velocities of  $\sim 2000 \text{ km s}^{-1}$  which are comparable to those of the optical ejecta knots [129]. Si, S, Ar, and Ca have similar general morphologies, but examination of their images in their line energies also show significant variations. At the positions of the brightest knots in the Si image at the inner boundary of the shell to the northeast and southeast the corresponding Ar and Ca X-ray images are much weaker in the remnant. Hughes et al [136] using the Chandra first light observation of Cas A ( $\sim 5000s$  on 1999 August 20) showed that the Fe-rich ejecta lie outside the S-rich material, and claimed that this is due to extensive, energetic bulk motions

which caused a spatial inversion of a part of the supernova core. However, on the basis of Spitzer Space Telescope imaging and spectral data Rudnick and collaborators [137], [133] claim that there are two roughly spherical shocks, (the blast wave and the reverse shocks) but “the wide spatial variations in composition seen in infrared, optical and X-ray studies are not due to local differences in ionization age or temperature, but instead reflect very specific asymmetries in the geometry of the underlying explosion. These asymmetries are ones in which the nucleosynthetic layers have remained mostly intact along each radial direction, but the velocity profiles along different radial directions vary over a range of approximately five” (see also [132]). In some directions, only the upper C-burning layers have been probed by the reverse shock, while in other directions, deeper O- and Si-burning layers have reached the reverse shock.

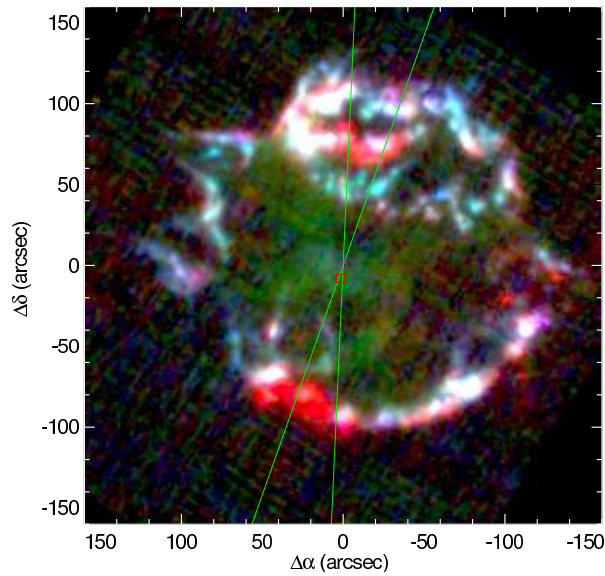


**Fig. 18.** Composite Spitzer image of Cas A in [Ar III] (blue), [S IV] (green), and [Ne II] (red), showing two pronounced neon-rich crescent-shaped regions to the N and S. The size of the image is  $320''$  with north to the top and east to the left. Shown are the kinematic center of the remnant at the magenta circle and X-ray localization of the remnant’s compact object (red square,  $7''$  to the south). Green lines indicate the  $1\sigma$  range of the “kick vector” direction of the compact object from the ejecta’s expansion center:  $169^\circ \pm 8.4^\circ$  [112]. The two regions of enhanced neon abundance lie very close to this projected direction. Several much smaller neon-enhanced regions lie in the West along the X-ray jet direction (Fig reproduced by permission of AAS and courtesy of J. Smith [133]).

The gas infrared lines of Ar, Ne, O, Si, S and Fe are seen at different locations, along with higher ionization states of the same elements visible in the optical and X-ray lines. For example, strong [Ar II] regions in the IR match very closely the places where helium- and hydrogen-like ionization states of Si and S are seen in the X-ray and [S III] seen in the optical [134]. These are the same regions with multiple temperatures and ionization states but show products of oxygen burning instead of carbon burning. Other regions, for example the crescent-shaped green feature slightly east of south in the Spitzer IRAC line and continuum images depicting gas in Fig 2 of [132] show strong [Ne II] emission in the IR (see also the red regions in the image Fig 18 reproduced from [133]), increasing [O III] emission in the optical and a gap in the silicon dominated X-ray emission, are interpreted as the locations where carbon-burning layers are presently encountering the reverse shock. Different layers containing various types of nucleosynthetic products seems to show the presence of characteristic types of dust, e.g. the deep layers contain silicates while the upper layers contain dust dominated by  $Al_2O_3$  and carbon grains. They also find evidence for circumstellar dust heated by the blast wave shock [137].

Smith et al [133] identify IR line emission from ejecta materials in the interior, prior to their encounter with the reverse shock, as well as from the post-shock bright ring. There is a dramatic increase in the electron density (by a factor  $\geq 100$  to  $\sim 10^4 \text{cm}^{-3}$ ) as well as a concomitant change in the ionization state of the ejecta as it encounters the reverse shock. There is a clear layering of ionization state, from low ionization species in the interior, e.g. [Si II] (8.2 eV), higher energies on the IR bright ring [S IV] (34.8 eV) where optical emission is also seen, and very high energies traced by X-ray line emission from H-like and He-like K-alpha resonance lines of Si XIII (0.5 keV) and Si XIV (2.4 keV), extending beyond the IR-bright rim. In addition, they find two compact, crescent shaped clumps with high neon abundance (mentioned above) which are arranged symmetrically around the central neutron star, and the crescent regions are closely aligned with the kick direction of the neutron star from the remnant's expansion center. These regions contain a huge amount of ionized neon (dominated by  $Ne^+$  and  $Ne^{++}$ , and excluding neutral neon), almost  $1.8 \times 10^{-4} M_\odot$ , flowing outwards  $\sim 20$  degrees from the plane of the sky at roughly  $-5500 \text{ km s}^{-1}$  in the south and  $+4200 \text{ km s}^{-1}$  in the north, while the entire SNR may contain an ionized neon mass  $\sim 8.6 \times 10^{-4} M_\odot$ . Smith et al comment that the *apparent* macroscopic elemental mixing mentioned in [136], may actually arise from different compositional layers of ejecta passing through the reverse shock at present along different directions.

### X-ray grating spectra of Cassiopeia A and SN 1987A

In the optical bands, thousands of individual knots have been observed to yield kinematic information, whereas the X-rays probe more dynamically important information since a much larger fraction of the ejecta mass is probed by X-rays

( $\sim 4M_{\odot}$  as compared to  $< 0.1M_{\odot}$  in the optical). The Chandra High Energy Grating Spectroscopy (HETGS) [131] provided for the first time the high spatial and spectral resolution X-ray map of Cas A, comparable to what is achievable in the optical. Because of Cas A's bright emission lines and narrow bright filaments and small bright clumps that stand out against the diffuse, continuum emission, this grating X-ray spectroscopy was possible and yielded rich information about the kinematic and plasma properties of the emitting knots. The HETGS has two grating arms with different dispersion directions, with the medium energy range (MEG) covering the range 0.4 – 5.0 keV and spectral FWHM of 0.023 Å, while the high energy range (HEG) covers 0.9 – 10.0 keV and spectral FWHM 0.012 Å. The grating spectra were obtained by Lazendic et al on some 17 different positions on the Cas A image, mainly near the reverse shock regions which are X-ray bright.

As mentioned already, Cas A image in the HETGS both in the non-dispersed (zeroth-order) as well as dispersed images in different energy bands contain H- and He-like ionization states of O+Ne+Fe (0.65-1.2 keV), Mg (1.25-1.55 keV), Si (1.72-2.25 keV), S (2.28-2.93 keV), Ar (2.96-3.20 keV), Ca (3.75-4.0 keV). In addition images in the Li- and Be-like states of Fe K lines (6.3-6.85 keV) are also obtained. A key advantage of high resolution grating spectroscopy over the low resolution “non-dispersive” CCD spectroscopy is that the former can be used to resolve individual lines and thereby interpret conditions in the radiating plasma in various parts of the SNR. The He-like ions of Si and S and other elements present in Cas A are the dominant ion species for each element over a wide range of temperatures and they emit strong K-shell lines of these ionic stages. For typical plasma densities in the SNR, the He-like triplet of Si and S lines shows strong forbidden (f) and resonance lines (r) and a comparatively weaker intercombination line (i) (see section 4.5 of [138] for an illustration of these transitions in O-ions). The G-ratio =  $(f+i)/r$  is, for example, a good diagnostic of the electron temperature [139]. Thus the measured line ratios and abundance ratios of H- and He-like ions of the same element (say Si) were used [131] to measure the electron temperature  $kT_e$  and the ionization time scale  $\tau = n_e t$  ( $n_e$  being the electron density and  $t$  being for example the time since the region was hit by the shock). The results of [131] show that for most of the selected regions, resolved spectroscopy of Si He-like triplet lines and Si H-like lines yields temperatures around  $\sim 1$  keV, consistent with reverse shocked ejecta. However, two regions, (designated R8 and R10) had significantly higher temperatures  $\sim 4$  keV, and could be part of the circumstellar material. The dominant element in Cas A seems to be Oxygen, and the electron density in the X-ray line emitting regions seem to vary between 20 to 200  $\text{cm}^{-3}$ , which is more typical of the unshocked interior of the IR line-emitting plasma, than that at the shock front as shown in [133] (see above). Lazendic et al had derived unambiguous Doppler shifts for their selected 17 regions. While the SE region of the SNR show mostly blue shifted velocities reaching upto  $-2500 \text{ km s}^{-1}$  (compare the IR line velocities in the south  $-5500 \text{ km s}^{-1}$ ), the NW side of

the SNR had extreme red shifted values up to  $+4000 \text{ km s}^{-1}$  (compare IR line velocity in the north:  $+4200 \text{ km s}^{-1}$ ).

Deep high resolution X-ray spectroscopy of SN 1987A was undertaken with Chandra HETG, 20 years after its explosion [140]. The impact of the SN ejecta with the circumstellar medium dominates the observed luminosity, the X-ray luminosity having brightened by a factor of 25 from that in 1999 and is presently increasing at the rate of 40 % per year [141]. An expanding elliptical ring is seen in the X-ray image whose brightness distribution seems to correlate with the rapidly brightening optical hot spots on the inner circumstellar ring observed with Hubble Space Telescope. The HETG spectrum for a total live time of 355 ksec shows H-like and He-like lines of Si, Mg, and Ne, and O VIII lines and bright Fe XVII lines. Fig. 19 taken from Dewey et al [140] shows the resolved Si and Mg triplets (r, i, and f lines); the data have similarity with model G-ratios  $(f + i)/r$  mentioned earlier. Since the dispersed X-ray spectrum is a convolution of the spatial structure of the X-ray image and the motion of the X-ray emitting gas, Chandra's sub-arc second resolution was important to resolve the circumstellar ring of dimensions  $1.2'' \times 1.6''$ .

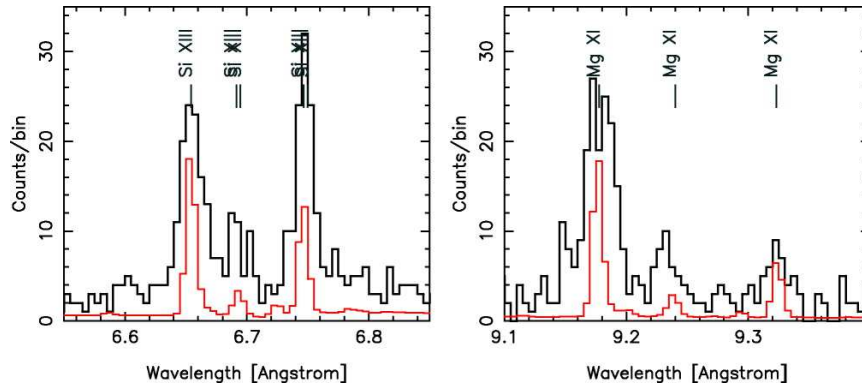


**Fig. 19.** Si (left panel) and Mg (right panel) triplets (resonance, intercombination and forbidden lines) resolved by Chandra High Energy transmission Grating Spectroscopy. The data are shown by the solid black histogram and an arbitrarily scaled point-source version of the two-shock model (no spatial-velocity effects) is shown in red to suggest the relative similarity of the data and model G-ratios  $[(f+i)/r]$ . (Fig reproduced by permission of the AAS and courtesy of D. Dewey [140]).

The global fit to the HETGS data with a two shock model yielded element abundances and absorption column densities which are consistent within the same 90% confidence limits that were derived from LETGS by [142]. The lower temperature shock seems to give the same  $kT_{low}$  for all the LETG data sets (in 2004 and 2007) and the HETG observation, whereas the  $kT_{high}$  values seem to show a general evolution towards lower values among the grating datasets and similar trend seen in the ACIS monitoring of SN 1987A.

The HETG data implies a relatively low bulk radial velocity of the shocked gas in the ring compared to model expectation from a plane parallel strong shock entering stationary gas and the temperature range inferred from the spectral modeling of the emitting gas. Since the X-ray image is correlated with the optical hot spots, it appears that the blast wave ahead of the SN ejecta is overtaking dense clumps of circumstellar gas in the hot spots. The blast wave may be encountering the dense clumps either at normal incidence or at oblique incidence. In the former case, the reflected shock would give rise to gas that has been shocked twice and having nearly stationary bulk velocity but further elevated temperature. With more and more X-ray emission coming from gas behind reflected shocks, there would be an increase of the fraction of higher temperature X-ray emission, consistent with what is seen. If the blast wave encounters dense clumps at an oblique incidence, the shocked gas will have significant velocity component parallel to the shock surface, and a significantly fast transmitted component emitting X-rays can result. The Doppler broadening seen in the line profiles of the Chandra data seems to suggest that both transmitted and reflected shocks encountering the circumstellar ring at normal and oblique angles may be at play [140].

## 10.2 Live radioactive decays in Cas A, SN 1987A

Gamma-ray, X-ray, optical and infrared line spectroscopy of SNe and SNRs have been used to observe nucleosynthesis and the abundance distribution of elements freshly synthesized (both radioactive isotopes and stable decay products) and to extract dynamical information about the explosion. In particular the radioactive isotopes provide unique tracers of nucleosynthetic processes (what, where and how much) and its related dynamics. The best examples are the observations of gamma-ray lines in supernovae, but X-ray line spectroscopy of decay products of radioactive nuclei have also been attempted, and specific elements in numerous SNRs and a few SNe identified.

After a few days, the main energy input to the SN ejecta comes from radioactive decay. For SN 1987A, at first, the important isotopes are  $^{56}\text{Ni}$  ( $\tau_{1/2} = 6.1d$ ) followed by  $^{56}\text{Co}$  ( $\tau_{1/2} = 78.8d$ ). Beyond  $\sim 1100$  days,  $^{57}\text{Co}$  is more important and at  $\geq 2000d$ , the dominant role is played by  $^{44}\text{Ti}$ . Using bolometric and broad-band UBVR light curves [143] estimated the masses of the three most important radio-isotopes in SN 1987A to be  $^{56}\text{Ni}(0.069 \pm 0.003M_{\odot})$ ,  $^{57}\text{Ni}(0.003M_{\odot})$  and  $^{44}\text{Ti}(1 \pm (0.5 - 2) \times 10^{-4}M_{\odot})$ .

Among the radioactive isotopes accessible to gamma-ray astronomy,  $^{44}\text{Ti}$  is a key isotope for the investigation of the inner regions of core collapse SNe and their young SNRs. It has a half-life of  $58.9 \pm 0.3$  yr [144] and a decay scheme:  $^{44}\text{Ti} \rightarrow ^{44}\text{Sc} \rightarrow ^{44}\text{Ca}$ . The discovery [145] of the 1157 keV gamma-ray line emission<sup>27</sup> from Cas A with the Compton Gamma Ray Observatory was the first direct proof of synthesis of this short lived, freshly

<sup>27</sup>  $J^{\pi} = 2^{+} \rightarrow 0^{+}$  transition in  $^{44}\text{Ca}$  reached from  $^{44}\text{Sc}$  following electron capture.

made radio-isotope in SNe. Renaud et al [146] using the INTEGRAL spacecraft recently reported the detection of both 67.9 and 78.4 keV gamma-ray lines of  $^{44}\text{Sc}$  in Cas A. There was a clear separation of the two lines due to an improved detection of the hard X-ray continuum up to 100 keV. The line flux of  $(2.5 \pm 0.3) \times 10^{-5} \text{ cm}^{-2} \text{ s}^{-1}$  leads to a tightly constrained  $^{44}\text{Ti}$  mass of  $(1.6_{-0.3}^{+0.6}) \times 10^{-4} M_{\odot}$ . This is actually high compared to the predictions of the standard models [135], [147], or their improved versions [148], [149]. Since the production of  $^{44}\text{Ti}$  is sensitive to the explosion energy and asymmetries and Cas A is known to be asymmetric and energetic ( $2 \times 10^{51}$  erg instead of the standard  $1 \times 10^{51}$  erg), this could be a factor in its apparent overproduction compared to models. At the same time, the recent revision of the  $^{40}\text{Ca}(\alpha, \gamma)^{44}\text{Ti}$  reaction rate [150] has led to an increase of  $^{44}\text{Ti}$  production by a factor of  $\sim 2$ .

Live radioactive isotopes freshly synthesized in the explosion were detected from SN 1987A by directly detecting 1238 keV and 847 keV gamma-ray lines [151], which provided detailed diagnostics of the nuclear burning conditions and the explosion dynamics. Another radio-nuclide  $^{57}\text{Co}$ , which is a decay product of  $^{57}\text{Ni}$  made in the supernova explosion, was also detected directly by measuring gamma-ray lines [152]. The calculated gamma-ray light curves for 847 keV and 1238 keV and other lines [153] could be made consistent with the Solar Maximum Mission (SMM) measurement only if the  $^{56}\text{Co}$  was mixed up to a mass coordinate of  $M_r \sim 13.5 M_{\odot}$ . The calculated fluxes were still slightly smaller than the observed fluxes at  $t \sim 200d$ , but this discrepancy could be removed by taking account of the effect of clumpiness in the ejecta which is more significant in the earlier phases. Also, the observed flux ratio between the two gamma-ray lines at 847 keV and 1238 keV is close to unity at early stages because of the smaller cross section for the 1238 keV lines than for 847 keV. As the column depth of the overlying matter decreased due to dilution with time in an expanding envelope, the observed flux ratio approached the expected value of 0.68 based on branching ratios [153].

X-ray fluorescence spectrometry technique has been used by archaeologists to determine the major and trace elements in ceramics, glass etc. Here, a sample is irradiated with X-rays and the wavelengths of the released (fluorescent) X-rays are measured. Since different elements have characteristic wavelengths, they can be identified and their concentrations estimated from the intensity of the released X-rays. Trace elements analysis may, for example, help in identifying the (geographical) source of a material. A similar method has been proposed [154] and attempted for SN 1987A [155]. It utilizes electron capture decays of freshly synthesized radio-nuclei. Following the electron capture, the K-shell vacancies are in most cases filled in by downward transitions from other bound shells. As the fluorescence X-ray yields are well known, measuring the X-ray line fluxes can then estimate the number of freshly synthesized nuclei. For example, attempts were made to detect the 5.9 keV  $\text{K}\alpha$  line from the stable nucleus  $^{55}\text{Mn}$  in the Chandra X-ray spectrum of SN 1987A, which is due to the decay of radioactive  $^{55}\text{Fe}$ . Both  $^{55}\text{Fe}(\tau_{1/2} = 2.7 \text{ yr})$  and

$^{55}\text{Co}$  ( $\tau_{1/2} = 18$  hr) are produced in explosive, incomplete Si burning as well as in normal freezeout of nuclear statistical equilibrium, in the inner ejecta of core collapse supernovae. However, no evidence of the 5.9 keV line emission from Mn could be found in 400 ks of Chandra ACIS data and the upper limit to the mean flux was  $< 3 \times 10^{-7} \text{ cm}^{-2}\text{s}^{-1}$ . Rauscher et al [148] calculated the ejected mass of  $A = 55$  radioactive nuclei to be  $7.7 \times 10^{-4} M_{\odot}$  for  $20M_{\odot}$  models of which most was  $^{55}\text{Co}$ . If only about half this mass of  $^{55}\text{Fe}$  were ejected, the reduced flux would be consistent with the observed upper limit. On the other hand the, even if the total mass inside were as much as  $1 \times 10^{-3} M_{\odot}$ , but the  $^{55}\text{Fe}$  abundance was zero outside the radial velocity shells at  $1500 \text{ km s}^{-1}$ , the line flux would be still consistent with data, as at late times the emerging flux depends sensitively on the presence of  $^{55}\text{Fe}$  in the outer zones.

### 10.3 Other X-ray supernovae

Apart from SN 1987A, which occurred close by and was therefore easy to detect, there are supernovae with relatively high intrinsic X-ray luminosity. SN 1993J and SN 1995N are two of them and they are at the high end of the X-ray luminosity [156], [157], which makes it suitable for study in the X-ray wave bands even at late stages [159]. Nymark et al [158] have shown that SNe with strong X-ray emission are likely to have radiative shocks and that in these shocks a large range of temperatures contribute to the spectrum. The cooling of the shock also affects the hydrodynamics of the flow structure and the volume of the emitting gas and thus the total luminosity from the interaction region. A shock is radiative depending on whether the cooling time scale  $t_{cool}$  of the shock is short compared to its expansion time  $t$ . Since the cooling function (from electron bremsstrahlung or free-free scattering and X-ray line emission from bound-bound transitions of ionized atomic species) is a function of the shock temperature this condition translates to a condition on the shock temperature for radiative vs. adiabatic shock. The boundary of the two regimes depends upon the shock velocity  $V_s$  and the ejecta density profile (given by the index  $\eta$  in  $\rho \propto v^{-\eta}$ ) and the separation in turn depends upon the chemical composition of the ejecta (see Fig. 20 reproduced from [160]). For a given shock velocity (and a composition and mass loss parameter of the progenitor stellar wind and the ejecta velocity scale), the shock is likely to be radiative for steeper density gradients.

As already mentioned, the spectroscopic type of SN 1993J from a type II-like SN at early times due to detected Balmer lines soon weakened and it came to resemble a type Ib SN, leading to a reclassification as a type IIb SN [161]. This transition is best explained if the progenitor star prior to its explosion, had lost its hydrogen envelope due to interaction with a binary companion [120], [121], [162], [163], [122]. If the H-envelope was indeed already thin, then the reverse shock would transit the H-rich region quickly, and soon the emission may be dominated by material dredged up from the nuclear processed parts of the star in the interior. In the 4H47 model of Shigeyama et al [164], by

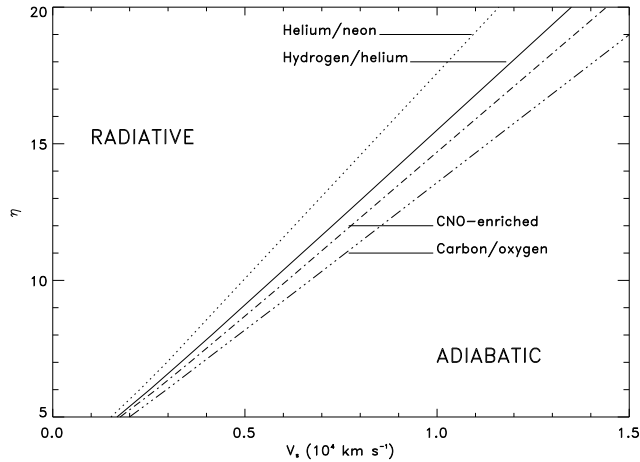


**Fig. 20.** The border between radiative and adiabatic regions of the shocks in supernovae as a function of shock velocity and ejecta density profile index  $\eta$  ( $\rho \propto v^{-\eta}$ ). The boundaries depend upon the composition of the ejecta through which the shock may be propagating as also the mass loss parameter of the progenitor stellar wind and the ejecta velocity scale (Fig. courtesy T. Nymark [160]).

2600 days after explosion, the hydrogen-rich envelope had  $\sim 0.47M_{\odot}$ . Inside this envelope is the outer part of the He-zone which is enriched in N (about  $\sim 0.3M_{\odot}$ ), while its inner part is C-rich (has  $\sim 1.5M_{\odot}$ ). If the circumstellar medium or the ejecta is clumpy, they may be hit by the reverse shock obliquely and the shock in the clump will be slower and the shock temperature lower. The presence of both hard X-rays and optical emission from the shocked CSM shows the importance of a clumpy CSM, for example in SN 1987A where a range of shock speeds are necessary to explain the observed spectrum [142]. SN 1993J is not as bright as SN 1987A or Cas A due to its larger distance, and both Chandra and XMM-Newton data is comparatively of a moderate signal to noise, at the low (CCD) resolution. The XMM spectrum of SN 1993J is dominated by the Fe L emission at 0.7 - 1.0 keV and is blended with strong Ne IX-X emission. Above 1.0 keV, emission lines which may be present are from Mg XI-XII, Si XIII-XIV, as well as S XVI. Nymark et al find that the spectrum of SN 1993J is fit best by a combination of an adiabatic shock ( $kT_{rev} = 2.1$  keV) propagating through a zone with CNO burning products, with He dominant and N and Ne being the most abundant metals, and a second radiative shock ( $kT_{rev} = 1.0$  keV). The latter could have been caused by instabilities at the reverse shock front or by a clumpy CSM. The XMM spectrum of SN 1993J and the model fits used [160] are shown in Fig 21.

SN 1995N is a type IIn supernova, a type that shows unusual optical characteristics and spans a very broad range of photometric properties such as

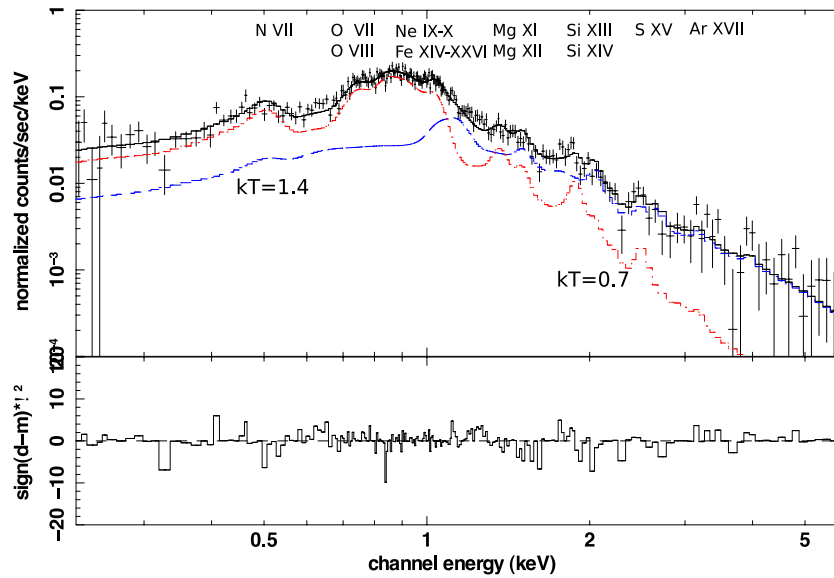


**Fig. 21.** XMM spectrum of SN 1993J (shown by data-points with crosses from April 2001). The data is fitted with an adiabatic shock at  $kT_{rev} = 2.1$  keV (long dashed in blue) and a radiative shock at  $kT_{rev} = 1.0$  keV (short dashed in red) for a He/N dominated composition from model s15s7b [163]. (Fig. courtesy T. Nymark [160]).

decline rates at late times [165]. It is likely that these differences are related to their progenitor's structure, mass, composition as well as the composition and the density profile of the CSM [166]. These supernovae show the presence of strong, narrow Balmer line emission on top of the broader emission lines in their early spectra. The narrow emission lines may originate in the dense and ionized circumstellar (CS) gas [167, 168]. The presence of strong  $H\alpha$  emission line, the high bolometric luminosity and the broad  $H\alpha$  emission base powered by the interaction of the supernova shock with the CSM, all point towards a very dense circumstellar environment [169]. When the stellar core collapses and explodes, the supernova lights up the slow-moving gas into narrow emission lines leading to the type II<sub>n</sub> supernova classification (n for narrow emission line). This interaction of the supernova shock with the dense CS gas is indicated by strong radio and X-ray emission detected from several type II<sub>n</sub> supernovae and in particular SN 1995N.

Chandra ACIS observations of SN 1995N show a best-fit line energy at 1.02 keV which is ascribed to Ne X [170]. There is also the possibility of another line with best-fit line energy at 0.85 keV with identification as Ne IX. The ionization potentials of all ionized Neon species upto Ne VIII are less than 240 eV, whereas those of Ne IX and Ne X are above 1195 eV. Hence at temperatures found by the Chandra observations, the predominant species of

Neon are expected to be Ne X and Ne XI. The mass of Neon was estimated to be about  $5 \times 10^{-3} M_{\odot} - 1 \times 10^{-2} M_{\odot}$ . This is consistent with Neon being in the Helium layer for a  $15 M_{\odot}$  star where it was co-synthesized with C, N, and He. For other stellar masses and other composition zones, the required Neon mass is much larger than observed. Therefore, Neon in the Helium core of the  $15 M_{\odot}$  star is the probable site where it was co-synthesized with C, N.

## Conclusions

Much insight about how stars burn nuclear fuel, evolve and ultimately explode has been obtained by calculations and computer simulations. Theoretical developments have been augmented by crucial astronomical observations over decades in all bands of electromagnetic radiation and through other signal channels like neutrinos. Most important have been the wider availability of powerful telescopes both from the ground and space platforms and state of the art computers. Crucial inputs to the field of nuclear astrophysics are also coming from laboratory experiments involving radioactive ion beams (RIB) and intense beams of energetic nucleons and nuclei. Short lived nuclei can only be studied close to their sites of formation in the laboratory before they decay. Such facilities will further advance the future of nuclear astrophysics.

## Acknowledgments

I thank Aruna Goswami and the organizers of the School for the invitation to Kodaikanal Observatory. Discussions with Katherina Lodders and Bruce Fegley at the School and Claus Rolfs and Richard McCray in other meetings are thankfully acknowledged. I thank Poonam Chandra and Firoza Sutaria for comments on this manuscript and for long term collaboration. Nuclear astrophysics research at Tata Institute is a part of the Plan Project: 11P-409.

## References

1. W. D. Arnett, *Supernovae and Nucleosynthesis*, Princeton University Press (1996)
2. M. N. Saha: Phil. Mag., **40**, 472 (1920)
3. M. N. Saha: Proc. Roy. Soc. Ser. A, **99**, 135 (1921)
4. H. Reeves, *Stellar Evolution and Nucleosynthesis*, Gordon and Breach, New York, (1968)
5. B. J. Carr, J. Bond, W. D. Arnett, ApJ **277**, 445 (1984)
6. B. J. Carr, ARAA **419**, 904 (1994)
7. W. Haxton, *Nuclear Astrophysics Course* (1999)  
<http://ewiserver.npl.washington.edu/phys554/phys554.html>

8. Oak Ridge National Lab, *Nuclear Data for Nuclear Astrophysics*  
<http://www.phy.ornl.gov/astrophysics/data>
9. Lawrence Berkeley National Lab, *Nuclear Astrophysics Reaction Rates*  
<http://ie.lbl.gov/astro/astrorate.html>
10. Joint Institute for Nuclear Astrophysics, *REACLIB library*  
<http://www.nscl.msu.edu/~nero/db>
11. Computational Infrastructure for Nuclear Astrophysics  
<http://www.nucastrodata.org>
12. M. S. Smith et al., in *CP1016, Origin of Matter and Evolution of Galaxies*, ed. by T. Suda et al., (AIP) p.466 (2008)
13. C. E. Rolfs, W. S. Rodney, *Cauldrons in the Cosmos*, University of Chicago Press (1988)
14. D. D. Clayton, *Principles of Stellar Evolution and Nucleosynthesis*, University of Chicago Press (1984)
15. J. N. Bahcall: *Neutrino Astrophysics*, Chapter 3, Cambridge University Press (1989); see also: <http://www.sns.ias.edu/~jnb/>.
16. R. N. Boyd *An Introduction to Nuclear Astrophysics*, University of Chicago Press (2008)
17. A. Ray, in *5th SERC School on Radioactive Ion Beams and Physics of Nuclei Away from the Line of Stability*, Chandigarh, ed. by I. M. Govil, R. K. Puri (Elite publishers, New Delhi), p. 99 (2003); arXiv:astro-ph/0405568.
18. A. V. Filippenko, in *Supernovae and Stellar Evolution, proceedings of the school and workshop in Goa*, ed. by A. Ray, T. Velusamy, World Scientific, Singapore, p 34 (1991)
19. R. P. Harkness, J. C., Wheeler, in *Supernovae*, ed. by A. Petschek, Springer, Berlin, p 1 (1990)
20. A. Goswami, N. Prantzos, *A&A* **359**, 191 (2000)
21. A. S. Eddington, *Observatory* **43**, 341 (1920)
22. R. d'E. Atkinson, F. G. Houtermans, *Z. Phys.* **54**, 656 (1929)
23. R. Davis, D. S. Harmer, K. C. Hoffman, *Phys. Rev. Lett.* **20**, 1205 (1968)
24. E. Rutherford: *Nature* **123**, 313 (1929)
25. T. Kirsten, in *The origin of the solar system*, ed. by S. F. Dermott, New York: Wiley, p 267 (1978)
26. W. A. Fowler, in *Proc. Welch Found. Conf. on Chemical Research*, ed. by W.D. Milligan, Houston Univ. Press, p 61 (1977)
27. H. A. Bethe, *Rev. Mod. Phys.* **9**, 69 (1937)
28. E. E. Salpeter, *Australian J. Phys.* **7**, 373 (1954)
29. R. Schiavilla, *Phys. Rev.* **C58**, 1263 (1998)
30. T. Itahashi et al, *Nucl. Phys.* **A718**, 466c (2003)
31. LUNA Collaboration, C. Casella, et al, *Nucl. Phys.* **A706**, 203 (2002)
32. C. F. von Weizsäcker, *Phys. Z.* **38**, 176 (1937)
33. C. F. von Weizsäcker, *Phys. Z.* **39**, 633 (1938)
34. H. A. Bethe, C. L. Critchfield, *Phys. Rev.* **54**, 248 (1938)
35. N. Christlieb et al., *Nature* **419**, 904 (2002)
36. J. N. Bahcall, M. C. Gonzalez-Garcia, C. Peña-Garay, *Phys. Rev. Lett.* **90**, 131301 (2003)
37. C. Peña-Garay, A. Serenelli, arXiv: 0811.2424 (2008)
38. W. Haxton, A. Serenelli, *ApJ* **687**, 678 (2008)
39. G. K. Schenter, P. Vogel, *Nucl. Sci. Engg.* **83**, 393 (1983)

40. E. Fermi, *Nuclear Physics, Course Notes*, University of Chicago Press, p 83 (1951)
41. H. A. Bethe, C. L. Critchfield, *Phys. Rev.* **54**, 862 (1938)
42. E. Frieman, L. Motz, *Phys. Rev.* **89**, 648 (1951)
43. E. E. Salpeter, *Phys. Rev.* **88**, 547 (1952); also *ApJ* **115**, 326 (1952)
44. J. N. Bahcall, R. M. May, *ApJ* **155**, 501 (1969)
45. H. A. Bethe, R. F. Bacher, *Rev. Mod. Phys.* **8**, 82 (1936)
46. J. N. Bahcall, C. P. Moeller, *ApJ* **155**, 511 (1969)
47. J. N. Bahcall, L. S. Brown, A. Gruzinov, R. F. Sawyer, *A. & A.* **383**, 291 (2002)
48. P. Quarati, A. M. Scarfone, *J. Phys. G.* **36**, 025203 (2009)
49. B. W. Filippone, et al., *Phys. Rev.* **C28**, 2222 (1983)
50. M. Gai, *Phys. Rev.* **C74**, 025810 (2006)
51. W. T. Winter et al, *Phys. Rev.* **C73**, 025503 (2006)
52. L. van Wormer et al., *ApJ* **432**, 326 (1994)
53. A. E. Champagne, M. Wiescher, *Ann Rev. Nucl. Part. Sci.* **42**, 39 (1992)
54. R. K. Wallace, S. E. Woosley, *ApJS*, **45**, 389 (1981)
55. M. Wiescher et al., *Prog in part & Nucl Phys.* **59**, 51 (2007)
56. C. Sneden, J. J. Cowan, R. Gallino, *ARAA* **48**, 241 (2008)
57. H. A. Bethe, *Phys. Rev.* **55**, 103 and 434 (1939)
58. E. J. Öpik: *Proc. Roy. Irish Acad.* **A54**, 49 (1951)
59. E. E. Salpeter, *Phys. Rev.* **107**, 516 (1957)
60. F. Hoyle, *ApJS* **1**, 121 (1954)
61. F. Hoyle, D. N. F. Dunbar, W. A. Wenzel, W. Whaling, *Phys. Rev.*, **92**, 1095 (1953)
62. C. W. Cook, W. A. Fowler, C. C. Lauritsen, T. Lauritsen, *Phys. Rev.* **107**, 508 (1957)
63. J. A. Nolen, S. M. Austin, *Phys. Rev.* **C13**, 1773 (1976)
64. C. Angulo, *Exp Tools for Nuclear Astrophysics*, *Lecture Notes in Physics* **764**, 253 (2009)
65. L. Buchmann, C. A. Barnes: *Nucl. Phys.*, **A777**, 254 (2006)
66. A. Lefebvre-Schuhl, in *Frontiers in Nuclear Structure, Astrophysics and Reactions: FINUSTAR 2*, ed. by P. Demetriou et al., (AIP), p 150 (2008)
67. S. E. Woosley, T. A. Weaver, *ARAA* **24**, 205 (1986)
68. C. Hayashi, R. Hoshi, D. Sugimoto, *Prog. Theor. Phys. Suppl.* **22**, (1951)
69. M. Mazarkis, W. Stephens, *ApJ* **171**, L97 (1972)
70. H. Reeves, E. E. Salpeter, *Phys. Rev.* **116**, 1505 (1959)
71. W. R. Hix, F. K. Thielemann, *ApJ* **460**, 869 (1996)
72. F. K. Thielemann, W. D. Arnett, *ApJ* **295**, 264 (1985)
73. G. M. Fuller, W. A. Fowler, M. J. Newman, *ApJ* **252**, 715 (1982)
74. K. Kar, A. Ray, S. Sarkar, *ApJ* **434**, 662 (1994)
75. J. -U. Nabi, M. Sajjad, *Phys. Rev.* **C77**, 055802 (2008)
76. K. Langanke, G. Martinez-Pinedo, *nucl-th/0203071*, *Rev. Mod. Phys.* **75**, 819 (2003)
77. W. R. Hix et al., *ApJ* **667**, 476 (2007)
78. H. Y. Chiu, *Ann of Phys* **15**, 1 (1961)
79. E. M. Burbidge, G. R. Burbidge, W. A. Fowler, F. Hoyle, *Rev. Mod. Phys.* **29**, 547 (1957)
80. G. Gamow, M. Schoenberg, *Phys. Rev.* **59**, 539 (1941)

81. S. E. Woosley, H. -T. Janka, *Nature Physics* **1**, 147 (2005)
82. H. A. Bethe, J. Wilson, *ApJ* **295**, 14 (1985)
83. H. A. Bethe, G. E. Brown, J. Applegate, J. Lattimer, *Nucl. Phys. A* **324**, 487 (1979)
84. W. D. Arnett, *ApJ* **218**, 815 (1977)
85. S. W. Bruenn, *ApJS* **58**, 771 (1985)
86. P. S. Joshi, *Scientific American* **300**, 36 (2009)
87. G. E. Brown, H. A. Bethe, G. Baym, *Nucl. Phys. A*, **375**, 481 (1982) (BBB)
88. G. M. Fuller, *ApJ* **252**, 741 (1982)
89. A. Ray, S. M. Chitre, K. Kar, *ApJ* **285**, 766 (1984)
90. H. A. Bethe, G. E. Brown, J. Applegate, J. M. Lattimer, *Nucl. Phys. A* **324** 487 (1979)
91. K. Kar, A. Ray, *Phys Lett* **96A**, 322 (1983)
92. A. Zaringhalam, *Nucl. Phys. A* **404**, 599 (1983)
93. F. K. Sutaria, A. Ray: *Phys. Rev.*, **C52**, 3460 (1995)
94. F. K. Sutaria, A. Ray, J. A. Sheikh, P. Ring, *A&A* **349**, 135 (1999)
95. O. Civitarese, A. Ray, *Physica Scripta* **59**, 352 (1999)
96. H.-T. Janka, K. Langanke, A. Marek, G. Martinez-Pinedo, B. Mller, *Phys. Rept.* **442**, 38 (2007)
97. A. F. Fantina, P. Donati, P. M. Pizzochero, *Phys. Lett.* **B 676**, 140 (2009)
98. D. J. Dean, K. Langanke, J. M. Sampaio, *Phys Rev.* **C66**, 45802 (2002)
99. F. K. Sutaria, A. Ray, *Phys. Rev. Lett.* **79**, 1599 (1997)
100. Sudbury Neutrino Observatory Proposal, SNO-87-12, October (1987)
101. J. N. Bahcall, K. Kubodera, S. Nozawa, *Phys. Rev.* **D 38** 1030 (1988)
102. A. S. Burrows, in *Supernovae*, ed. by A. G. Petschek, Springer-Verlag (1990)
103. L. M. Segal, *Nucl. Phys.* **B 70**, 61 (1974)
104. T. Weaver, S. E. Woosley, G. M. Fuller, *Nuclear Astrophysics: Essays in honor of J. Wilson*, ed. by J. Centrella et al., 374 (1985)
105. R. M. Bionta et al., *Phys. Rev. Lett.*, **58**, 1494 (1987) (IMB collaboration)
106. K. Hirata, et al., *Phys. Rev. Lett.* **58**, 1490 (1987) (KII collaboration)
107. W. D. Arnett, J. N. Bahcall, R. P. Kirshner, S. E. Woosley, *ARAA* **27**, 629 (1989)
108. D. Casper, *UNO A Next Generation Detector for Nucleon Decay and Neutrino Physics*  
meco.ps.uci.edu/lepton\_workshop/talks/casper/uno.pdf (2000).
109. K. J. Chang, *hep-ex/0005046* (2000)
110. R. A. Chevalier, C. Fransson, in *Supernovae and Gamma-Ray Bursters*, ed. by Kurt Weiler, *Lecture Notes in Physics*, 598, 171 (2003)
111. S. Immler, W. H. G. Lewin, in *Supernovae and Gamma-Ray Bursters*, ed. by Kurt Weiler., *Lecture Notes in Physics*, vol. 598, p. 91 (2003)
112. R. A. Fesen et al., *ApJ* **645**, 283 (2006)
113. J. E. Reed, J. J. Hester, A. C. Fabian, P. F. Winkler, *ApJ* **440**, 706 (1995)
114. M. Ryle, F. G. Smith, *Nature* **162**, 462 (1948)
115. S. P. Reynolds, *ARAA* **48**, 89 (2008)
116. O. Krause et al., *Science* **320**, 1195 (2008)
117. S. E. Woosley, N. Langer, T. A. Weaver, *ApJ* **411**, 823 (1993)
118. G. Aldering, R. M. Humphreys, M. Richmond, *AJ* **107**, 662 (1994)

119. N. Rathnasree, A. Ray, *JAA* **13**, 3 (1992)
120. A. Ray, K. P. Singh, F. K. Sutaria, *JAA* **14**, 53 (1993)
121. K. Nomoto et al., *Nature* **364**, 507 (1993)
122. J. R. Maund, S. J. Smartt, R. P. Kudritzki, P. Podsiadlowski, G. F. Gilmore, *Nature* **427**, 129 (2004)
123. T. Matheson et al., *AJ* **120**, 1487 (2000)
124. R. A. Chevalier, J. Oishi, *ApJ* **593**, L23 (2003)
125. C. Fransson, P. Lundqvist, R. A. Chevalier, *ApJ* **461**, 993 (1996)
126. P. Chandra, A. Ray, S. Bhatnagar, *ApJ*, **612**, 974 (2004)
127. R. A. Fesen, K. S. Gundersen, *ApJ* **470**, 967 (1996)
128. U. Hwang et al., *ApJ* **615**, L117 (2004)
129. U. Hwang, S. S. Holt, R. Petre, *ApJ* **537**, L119 (2000)
130. R. Willingale et al., *A&A* **381**, 1039 (2002)
131. J. S. Lazendic, D. Dewey, N. S. Schulz, C. R. Canizares, *ApJ* **651**, 250 (2006)
132. J. A. Ennis et al., *ApJ* **652**, 376 (2006)
133. J. D. T. Smith et al., *ApJ* **693**, 713 (2009)
134. R. A. Fesen et al., *AJ* **122**, 2644 (2001)
135. S. E. Woosley, T. A. Weaver, *ApJS* **101**, 181 (1995)
136. J. P. Hughes et al., *ApJ* **528**, L113 (2000)
137. L. Rudnick, in *The 10th International Symposium on Origin of Matter and Evolution of Galaxies, Sapporo, Japan*, ed. by Takuma Suda et al., AIP Conference Proceedings, Volume 1016, p. 353 (2008)
138. D. A. Liedahl, in *X-ray Spectroscopy in Astrophysics, X EADN School Amsterdam*, ed. by J. van Paradijs, J. A. M. Bleeker, Springer, Berlin, 189 (1999)
139. D. Porquet et al., *A&A* **376**, 1113 (2001)
140. D. Dewey, S. A. Zhekov, R. McCray, R. Canizares, *ApJ* **676**, L131 (2008)
141. S. Park et al., in *Supernova 1987A: 20 Years After*, ed. by S. Immler, K. W. Weiler, R. McCray (New York: AIP) 43 (2007)
142. S. A. Zhekov et al., *ApJ* **645**, 293 (2006)
143. C. Fransson, C. Kozma, *New Astron Rev.* **46**, 487 (2002)
144. I. Ahmad et al., *Phys. Rev.* **C74**, 065803 (2006)
145. A. F. Iyudin et al., *A&A* **284**, L1 (1994)
146. M. Renaud et al., *ApJ* **647**, L41 (2006)
147. F. K. Thielemann, K. Nomoto, M. Hashimoto, *ApJ* **460**, 408 (1996)
148. T. Rauscher et al., *ApJ* **576**, 323 (2002)
149. M. Limongi, A. Chieffi, *ApJ* **592**, 404 (2003)
150. H. Nassar et al., *Phys. Rev. Lett.* **96**, 041102 (2006)
151. S. M. Matz et al., *Nature* **331**, 416 (1988)
152. J. D. Kurfess et al., *ApJ* **399**, L137 (1992)
153. K. Nomoto et al., in *Supernovae and Stellar Evolution, proceedings of the school and workshop in Goa*, ed. by A. Ray, T. Velusamy, World Scientific, Singapore p. 116 (1991)
154. M. D. Leising, *New Astr. Reviews* **46**, 529 (2002)
155. M. D. Leising, *ApJ* **651**, 1019 (2006)
156. H. U. Zimmermann, B. Aschenbach, *A&A* **406**, 969 (2003)
157. D. W. Fox, et al., *MNRAS* **319**, 1154 (2000)
158. T. Nymark, C. Fransson, C. Kozma, *A&A* **449**, 171 (2006)

159. P. Chandra et al., *ApJ* **699**, 388 (2009)
160. T. Nymark, P. Chandra, C. Fransson, *A&A* **494**, 179 (2009)
161. A. V. Filippenko, T. Matheson, L. C. Ho, *ApJ* **415**, L103 (1993)
162. Ph. Podsiadlowski et al., *Nature* **364**, 509 (1993)
163. S. E. Woosley et al., *ApJ* **429**, 300 (1994)
164. T. Shigeyama et al., *ApJ* **420**, 341 (1994)
165. A. V. Filippenko, *ARAA* **35**, 309 (1997)
166. W. Li, A. V. Filippenko, S. D. Van Dyk, J. Hu, *PASP* **114**, 403 (2002)
167. R. B. C. Henry, D. Branch, *PASP* **99**, 112 (1987)
168. A. V. Filippenko, in *Supernova 1987A and other supernova, ESO Conference and Workshop*, ed. by J. Danziger and Kurt Kjaer, p 343 (1991)
169. N. N. Chugai, I. J. Danziger, *Astron. Lett.* **29**, 649 (2003)
170. P. Chandra et al., *ApJ* **629**, 933 (2005)